Journal of Computational Physics **183,** 577–622 (2002)
doi:10.1006/jcph.2002.7202

On a Wavelet-Based Method for the Numerical Simulation of Wave Propagation

Tae-Kyung Hong and B. L. N. Kennett

Research School of Earth Sciences, Institute of Advanced Studies, The Australian National University, Canberra, ACT 0200, Australia
E-mail: tkhong@rses.anu.edu.au, brian@rses.anu.edu.au

Received May 18, 2001; revised September 4, 2002

A wavelet-based method for the numerical simulation of acoustic and elastic wave propagation is developed. Using a displacement-velocity formulation and treating spatial derivatives with linear operators, the wave equations are rewritten as a system of equations whose evolution in time is controlled by first-order derivatives. The linear operators for spatial derivatives are implemented in wavelet bases using an operator projection technique with nonstandard forms of wavelet transform. Using a semigroup approach, the discretized solution in time can be represented in an explicit recursive form, based on Taylor expansion of exponential functions of operator matrices. The boundary conditions are implemented by augmenting the system of equations with equivalent force terms at the boundaries. The wavelet-based method is applied to the acoustic wave equation with rigid boundary conditions at both ends in 1-D domain and to the elastic wave equation with a traction-free boundary conditions at a free surface in 2-D spatial media. The method can be applied directly to media with plane surfaces, and surface topography can be included with the aid of distortion of the grid describing the properties of the medium. The numerical results are compared with analytic solutions based on the Cagniard technique and show high accuracy. The wavelet-based approach is also demonstrated for complex media including highly varying topography or stochastic heterogeneity with rapid variations in physical parameters. These examples indicate the value of the approach as an accurate and stable tool for the simulation of wave propagation in general complex media.

Key Words: acoustic; elastic; wave propagation; numerical simulation; wavelets; semigroup formulation; operator representation; topography; grid generation; complex media.

0021-9991/02 $35.00

1. INTRODUCTION

1.1. Previous Wavelet-Based Techniques and Motivation of This Study

The discrete wavelet transform [20] has become a powerful tool in signal analysis because wavelets are confined in both the frequency and time domains. The transformation is based on a multiresolution analysis that projects a signal onto successive wavelet subspaces representing different scales of variation.

Applications of wavelets have been made for several aspects of seismic signal processing such as the determination of an onset time of specific phase's arrival [2, 73], measurement of an anisotropy rate in certain regions [5], and estimation of a time varying spectral density matrix [52]. However, the applications of wavelets are not restricted to signal processing and have been extended to numerical analysis as well exploiting the adaptivity, compactness achievable in the wavelet domain. Lewalle [51] has exploited an explicit approach for certain classes of problem by a choice of wavelets which can be matched to the appropriate equations. He has applied Hermitian wavelets, the derivatives of a Gaussian bell-shaped curve, to a diffusion problem through a canonical transformation and showed a promising development for the numerical prediction of intermittent and nonhomogeneous phenomenon.

The adaptivity of wavelets has been one of the major motivations for the implementation of wavelets in numerical analysis [27, 33, 53]. Holmström [33] has implemented a composite technique to use the Deslauriers and Dubuc interpolating wavelets (DD wavelets; see [21, 22]) as a supplementary method for an usual finite difference (FD) scheme, so that he could reduce the computational cost in FD computation by imposing a threshold on the size of wavelet coefficients. However, the composite scheme does not escape the problems inherent in FD methods, for example, accumulation of errors across the grid.

Lippert *et al.* [53] have implemented a similar approach based on the adaptivity of DD wavelets in solving a Poisson equation. They have tried to represent physical operators (differential operators) in multilevel spaces based on DD wavelets. With the help of the adaptive scheme they could solve a problem having local nonlinear couplings in domain with given accuracy (or resolution) and less computational labour compared to nonadaptive full-grid based methods. The adaptive approach to parabolic equations may have difficulties with transient nonlinear phenomena because of the need to continually update the operators at each time step.

Fröhlich and Schneider [27] have applied wavelets to obtain numerical solutions of a reaction-diffusion system in one- and two-dimensional spaces and they have also used the adaptivity of wavelets for space discretization. They have been able to incorporate inherently periodic boundary conditions in special cases such as an outward burning flame. However, many natural phenomena do not satisfy periodic boundary conditions (e.g., adiabatic reactions at the boundaries) and then it is difficult to use such a wavelet-based method.

Qian and Weiss [61] have applied the wavelet-Galerkin method to obtain numerical solution of PDEs, especially boundary value problems (e.g., Helmholtz equation) in nonseparable domains. With the introduction of an 'extensive wavelet-capacitance matrix technique' which shows fast convergence at relatively coarse levels of discretization, they have been able to handle the boundary geometry effectively. Cai and Wang [14] have demonstrated the applicability of adaptive wavelet collocation methods using cubic splines for linear and nonlinear hyperbolic PDEs with initial boundary conditions in 1-D spatial domain. We note that Cai and Wang have introduced different shapes of wavelets and scaling functions for internal

and boundary regions, and could treat the boundary effects correctly without contaminating other regions. Dahmen [18] has reviewed basic theories of the wavelet-based scheme and adaptive techniques for numerical simulation for elliptic and parabolic problems.

Recently some numerical analysis based on wavelets has been applied in modelling of geophysical problems. In [74] the adaptive multilevel wavelet collocation method has been implemented in modelling of viscoelastic plume-lithosphere interaction by solving the partial differential equations representing viscoelastic flows with localized viscosity variations. Also, Rosa *et al.* [62] have demonstrated that a wavelet transform could be used to model static physical quantities in elastic media (e.g., displacement and stress fields) with consideration of boundary conditions.

So far the adaptivity which leads to a reduction in computational labour and in memory use via grid adaptation or wavelet-scale adaptation has been one of most attractive reasons for the use of wavelet-based scheme in numerical studies. However, the grid-adaptivity can be considered only in a limited way for a time-dependent PDE system due to constraints on the spatial grid steps for stable and accurate computation, for instance, the relationship to the slowest wave speed in wave propagation modelling (see Section 5.6). Also, the wavelet-scale adaptivity cannot be applied properly when the target vector has a broad frequency content, e.g., a wavefield composed by various scattering waves.

Another important aspect is that a wavelet scheme can represent the action of operator with high accuracy and stability through projection technique onto wavelet-based subspaces with compact support as a basis (e.g., Daubechies wavelets [7], B-spline wavelets [36]). Especially for time-dependent PDEs (e.g., wave equations), high accuracy in numerical differentiation is essential since this factor is directly related to the confidence of the numerical results and also in the reduction of computational load through implementation of larger spatial grid steps and larger time steps (see Section 5.6). For this purpose, the Fourier method [46], which can in principle achieve high accuracy in numerical differentiation, has been introduced in seismological modelling studies. However, the Fourier method often runs into difficulties in incorporating physical boundary conditions (e.g., vanishing tractions). The Chebychev-pseudospectral method [15, 47] could reduce such problems by introducing a Chebychev method for the vertical derivatives needed in the boundary condition.

We show that a wavelet-based method can give not only high accuracy in numerical differentiation but also flexible implementation of physical boundary conditions in the modelling of acoustic and elastic wave propagation. We exploit the use of a nonstandard form (*NS*-form) of matrix representation based on the works of Beylkin [7, 8], with extension to separable multidimensional operators (e.g., 2-D spatial partial derivatives in this study).

1.2. Methods for Modelling of Wave Propagation

A number of different methods have been applied to the numerical simulations of wave propagation in general complex media, such as finite difference, pseudospectral and spectral element methods. The finite difference method (FDM) has a long history in numerical modelling of wave propagation and has been steadily improved (e.g., [4, 31, 39, 57, 75]) with implementation to various studies (e.g., [25, 26, 76]) since the method is relatively easy for code development and needs relatively small computer memory. However, the FDM has difficulty in treating a free surface with topography or internal irregular boundaries (e.g., see [55, 56]); to treat this sort of problem, a hybrid technique implementing additional favorable method

(e.g., finite element method) supplementarily has been introduced (see [56]). Also, FDM has a tendency that numerical errors are accumulated across the grid during computation.

The pseudospectral method [3, 47] based on Chebychev expansions can provide higher accuracy spatial differentiation than simple FDM by using a series of global, infinitely differentiable basis functions. Also, this method distributes the error throughout the whole domain unlike usual grid-based methods such as FDM. This style of computation can achieve good results with fewer grid points per wavelength than FDM but care needs to be taken to avoid grid dispersion from implementation of nonuniform sampling grid system for the collocation points of the basis functions.

The spectral element method (SEM) has been introduced relatively recently for the modelling of elastic wave propagation [23, 45]. By including both the boundary conditions and force terms in a variational form of the governing equations and using element interaction, the SEM satisfies the free surface boundary condition implicitly and thereby avoids the complications for the implementation of boundary conditions encountered in other methods. Generally, the SEM can generate accurate modelling for most solid elastic media. However, for a fluid–solid layered medium problem, the method needs a special formulation of governing equations in terms of displacements in the solid region and velocity potential in the fluid region, and an explicit conditional time stepping should be applied (see [43]) for stable and accurate modelling. Therefore, the SEM computational procedure becomes more complex and is difficult to use for such cases as random media, the presence of a fluid-filled cavity, or an inhomogeneous fluid layer. We note that FDM also has some difficulty in treatment of liquid–solid interfaces and therefore needs special computational boundary conditions at the interfaces (see [68]).

In seismological studies, the complexity of earth processes heads to the need for stable and accurate modelling of elastic wave propagation media with randomly distributed cavities (or cracks) or in stochastic random heterogeneous media. However, current existing methods have some limitations in the treatment of such media. The FDM cannot generate an accurate response for a medium with highly varying physical parameters because of the limited accuracy of differentiation (see [35]) and strong numerical dispersion. Also, the Chebychev-pseudospectral method has a difficulty in treatment of random heterogeneity inside a medium due to its uneven grid steps. In the same way, it is difficult to design a mesh for stochastic heterogeneous media for SEM and also difficult to implement the presence of fluid-filled cavities media. In this circumstance, we develop a wavelet-based method for a stable and accurate computation in general complex media.

1.3. Development of a Wavelet Approach for Wave Propagation

We have adapted the approach introduced by Beylkin [9] for parabolic PDEs to the hyperbolic wave equation system by rewriting the governing equations in the form of a set of equations involving first-order derivatives in time. This can be achieved by working in terms of displacements and velocities with a consequent reduction in memory of about 30% compared to the more common velocity-stress formulation (e.g., [15, 45, 75]). The time evolution of the differential equations is achieved with an explicit scheme and a local Taylor expansion that allows us to make an effective representation of both vector and matrix operators involving spatial derivatives in terms of scalar wavelet components (Section 4.1).

Externally imposed boundary conditions such as the termination of a string or the free surface boundary condition of vanishing traction for elastic media need to be incorporated in

the wave propagation scheme. We are able to handle such conditions with the use of equivalent force systems applied at the material boundaries. Attenuation is built into the governing equations and so absorbing boundary conditions at appropriate edges of the domain can be introduced by raising the level of attenuation in those regions. The implementation of the boundary conditions are discussed in Section 5.3.

Because of the high accuracy of the representation of spatial differential operators, the wavelet scheme can be applied to wave propagation problems in complex structures. In [34] we have demonstrated the way in this scheme can be used when the physical parameters are varying with depth or distance. Here we focus on the applicability of a wavelet-based method in media with surface topography or complex internal heterogeneity. We illustrate elastic wave propagation in a homogeneous medium with sinusoidal topography at the free surface (Section 6.4) and in a stochastic heterogeneous medium with a fluid-filled crack (Section 6.5).

2. REPRESENTATION OF THE DIFFERENTIAL OPERATORS IN WAVELET BASES

We have used a representation of the action of differential operators through a wavelet based on the work of Beylkin [7], using Daubechies wavelets [20]. In this section, we briefly review the ideas for the representation of operators in wavelet bases in nonstandard form (*NS*-form [7]) and set out the notation for the extension of the work. We use the terminology 'matrix operator' for the representation of an operator decomposed using wavelet bases in the form of a matrix, as distinct from an 'operator matrix' (e.g., Eq. (36)) with action on a vector in physical space.

In the multiresolution analysis, each scaling subspace $\mathbf{V}_j$ ($j \in \mathbb{Z}$) is contained in spaces on lower scales such as

$$\{0\} \to \cdots \mathbf{V}_2 \subset \mathbf{V}_1 \subset \mathbf{V}_0 \subset \mathbf{V}_{-1} \subset \mathbf{V}_{-2} \cdots \to \mathbf{L}^2(\mathbf{R}), \tag{1}$$

where $\{0\}$ is a null space. The scaling subspace $\mathbf{V}_j$ can be decomposed into higher wavelet and scaling subspaces ($\mathbf{W}_{j+1}, \mathbf{V}_{j+1}$) using tensor product bases (φ, ψ, e.g., Daubechies wavelets; Fig. 1) at scale $j+1$, and thereby the scaling subspace can be decomposed successively up to a null space. Therefore, $\mathbf{L}^2$ space can be represented with a direct sum of wavelet subspaces, and any operator defined in $\mathbf{L}^2$ space can be potentially represented via projections of the operator onto subspaces. Since data (e.g., displacement field in domain) are collected discretely in a domain, the physical (numerical) space need not be an actual $\mathbf{L}^2$ space. We set the physical space to be $\mathbf{V}_0$, and an operator T defined in $\mathbf{L}^2$ space is considered as T_0 in the physical space $\mathbf{V}_0$.

When the operator T_0 is considered through effects on subspaces up to scale J, components of the matrix operator in standard wavelet form occur in 'finger' bands due to cross scale projections of an operator among subspaces, even from wavelet subspace to scalar subspace and vice versa (see [7]). With this form of matrix operator with a dense population of components, the computation cost increases dramatically as the scale J is increased. To reduce this huge computational labour and thereby increase efficiency, Beylkin [7] has considered an additional projection on to the set of subspaces ($\mathbf{W}_j, \mathbf{V}_j$, $j = 1, 2, \ldots, J$). With this further projection the matrix operator is reformulated as a sparse matrix where the non-zero components form submatrices arranged diagonally. We describe the details of the procedure for formulating matrix operators in *NS*-form in Appendix A, and for the application of the matrix operator to a vector in Appendix B.

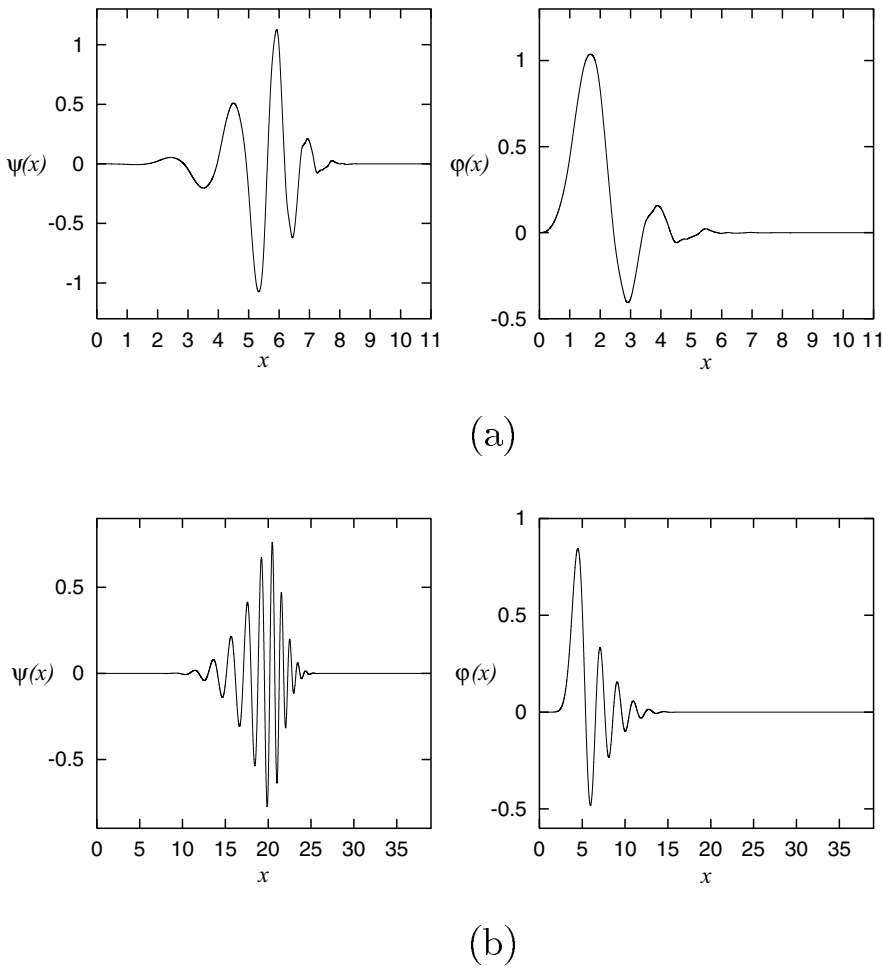

FIG. 1. Examples of wavelet $\psi(x)$ and its scaling function $\varphi(x)$ of Daubechies; (a) Daubechies-6 wavelets and (b) Daubechies-20 wavelets.

Since scalar differential operator for one-dimensional space [7] is implemented for a representation of vector (multispatial) differential operator (e.g., $\partial_z \partial_x u_x$), the vectors where the operator is applied have a directional character. As shown in Fig. 2, by collecting a vector in a given direction (i.e., horizontal direction, pth row; vertical direction, qth row) from a target vector field (e.g., displacement field), we can implement the directionality of the partial differential operators. So, when a operator $\partial_z \partial_x$ is applied to a displacement field u in a two-dimensional space, we apply a derivative operator to a horizontally sampled displacement vector and then a derivative operator to a vertically sampled vector from a $\partial_x u$ field.

During multispatial differentiation through a successive directed one-dimensional differentiation using wavelets, the size of each side $(x, y, z, \ldots)$ of domain is assumed to be same (namely, $0 < x, y, z, \cdots \leq 1$) regardless of number of data (i.e., grid points) employed. Therefore, a scaling process is needed to maintain the integrity of numerical modelling when there are different sizes of the edges of the domain. For example, when a 2-D spatial domain with size $(0 < x \leq 1, 0 < z \leq 2)$ is composed of $N \times M$ grid points and a cross

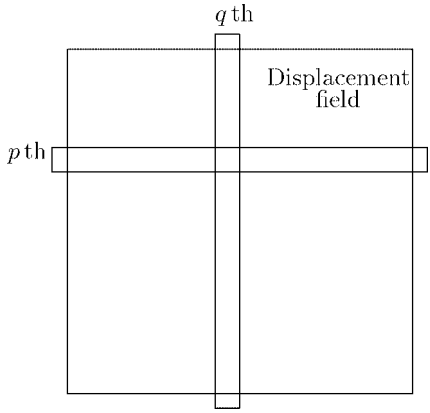

FIG. 2. Sampling in a displacement field.

partial differentiation operator $\partial_z \partial_x$ is implemented to a displacement field u, the vectors need to be multiplied by the relative size coefficient r_j (=reference length/j directional length, $j = x, z$) after each directional differentiation (e.g., $r_x = 1$, $r_z = 1/2$). Note that the actual values of N and M (or, grid spatial steps dx and dz) are not significant in this scaling procedure. However, the implementation of large enough N and M to achieve accurate (or stable) numerical differentiation of vectors is an important point considered for modelling of wave propagation (see Section 5.6).

3. SEMIGROUP APPROACH AND DISCRETE TIME SOLUTION

Using a displacement-velocity formulation and considering the time-independent spatial derivatives as linear operators (e.g., $\mathcal{L}$ in Eq. (8) or $\mathcal{L}_{ij}$ in (33)) which consist of an operator matrix (e.g., $\mathbf{L}$ in Eq. (9) or (36)), we can rewrite the wave equations as a first-order PDE system in time. We are then able to adapt the technique using a semigroup approach in [9] for the solution of the equation system.

Now we consider a discrete time solution of a set of first-order PDEs for evolution of a system in time using the semigroup approach. First, we consider a system of PDEs with an unknown $g(x, t)$ depending on the variables (x, t), which is composed of a linear part $\mathcal{L}g$ and a nonlinear 'forcing' term $\mathcal{N}f(g)$. Then

$$\partial_t g = \mathcal{L}g + \mathcal{N}f(g), \tag{2}$$

with an initial condition,

$$g(x, 0) = g_0(x), \quad 0 \le x \le 1. \tag{3}$$

Here $\mathcal{L}$ is a linear operator, $\mathcal{N}$ is a nonlinear operator and $f(g)$ is a nonlinear function of $g(x, t)$. Using a semigroup approach, the solution of this initial value problem (2) can be represented as the sum of an exponential function of the linear operator and a nonlinear integral function in time (see [6]):

$$g(x, t) = e^{t\mathcal{L}} g_0(x) + \int_0^t e^{(t-\tau)\mathcal{L}} \mathcal{N}f(g(x, \tau))\, d\tau. \tag{4}$$

This expression for $g(x, t)$ in (4) provides direct dependence on the initial conditions and provides for the existence and uniqueness of solutions.

When a solution $g(x, t)$ in (4) is considered at a discrete time in a numerical computation, the magnitude of the nonlinear integral function in (4) is approximated by an estimate based on an asymptotic analysis using the exact values from the linear part. The resultant discretization formula is given by (see [10])

$$g_{n+1} = e^{\delta t \mathcal{L}} g_n + \delta t \left(\gamma N_{n+1} + \sum_{m=0}^{R-1} \beta_m N_{n-m} \right), \tag{5}$$

where the coefficients γ and β_m are functions of $\delta t \mathcal{L}$, γ determines the nature of the scheme (implicit or explicit), β_m controls the order of a quadrature approximation, g_n is a function of $g(x, t)$ at the discrete times $t_n = t_0 + n\delta t$, δt is a time step and N_n is a nonlinear part at t_n. For a given R in (5), the order of accuracy is R for an explicit scheme and $R + 1$ for an implicit scheme. Since the terms considered at the positions for nonlinear forcing terms in this study (i.e., body force terms and explicit boundary conditions) are independent of unknown variables at previous discrete times, we set $R = 1$ and consider an explicit scheme ($\gamma = 0$) throughout the study.

The operator exponential $e^{\delta t \mathcal{L}}$ in (5) can be represented directly by the scheme in Appendix A for 1-D situation with one scalar unknown. When a vector unknown is implemented (e.g., $\mathbf{U}$ in (21), (35)) through a first-order PDE system for acoustic or elastic wave equations, the exponential is a function of an operator matrix $\mathbf{L}$ and can be represented properly using the scalar wavelet basis by augmenting a Taylor expansion. In acoustic and elastic wave situations we treat physical boundary conditions by introducing equivalent forces which are not continuous in $\mathbf{L}^2$ due to spatially localized nature of boundaries on the domain. We introduce both source terms (e.g., body forces) and the equivalent boundary terms by using suitable 'forcing' terms in (2). This enables the discrete time solution (5) to be used for wave propagation. When various boundary conditions and nonlinear effects are considered at every time step in a domain, the consideration via a set of forcing terms can increase the efficiency of computation and can reduce the numerical instability (e.g., [10, 34]).

We discuss detailed schemes for the acoustic and elastic wave equations in Sections 4.1 and 5.1. Also note that we consider relationships between the truncation order (i.e., maximum order of term considered) in the Taylor expansion and the discrete time step in Section 5.6.

4. ACOUSTIC WAVE EQUATION

4.1. Numerical Formulation

First, we consider an acoustic wave equation in one space dimension without any forcing term: for a uniform medium

$$\frac{\partial^2 u}{\partial t^2} = c^2 \frac{\partial^2 u}{\partial x^2}, \tag{6}$$

with initial conditions

$$u(x, 0) = u_0(x), \quad v(x, 0) = v_0(x), \tag{7}$$

where c is a wave velocity in a space. $u(x,t)$ and $v(x,t)$ are the components of displacement and velocity at a point x and time t.

In order to apply the semigroup approach to the wave equation, we rewrite (6) as a first-order differential equation system in time

$$\frac{\partial}{\partial t}\begin{pmatrix} u \\ v \end{pmatrix} = \begin{pmatrix} 0 & I \\ \mathcal{L} & 0 \end{pmatrix}\begin{pmatrix} u \\ v \end{pmatrix}, \tag{8}$$

where the linear operator $\mathcal{L}$ is $c^2\partial_x^2$. Here, we set the operator matrix $\mathbf{L}$ to be

$$\mathbf{L} = \begin{pmatrix} 0 & I \\ \mathcal{L} & 0 \end{pmatrix}. \tag{9}$$

Then through a semigroup approach, we can represent a solution of (6) as

$$\begin{pmatrix} u_{n+1} \\ v_{n+1} \end{pmatrix} = e^{\delta t\mathbf{L}}\begin{pmatrix} u_n \\ v_n \end{pmatrix}, \tag{10}$$

where u_n is a displacement component at discretized time t_n and v_n a velocity component. $e^{\delta t\mathbf{L}}$ is approximated using a Taylor expansion,

$$e^{\delta t\mathbf{L}} = \mathbf{I} + \delta t\mathbf{L} + \frac{\delta t^2}{2!}\mathbf{L}^2 + \frac{\delta t^3}{3!}\mathbf{L}^3 + \frac{\delta t^4}{4!}\mathbf{L}^4 + \cdots, \tag{11}$$

where $\mathbf{I}$ is a 2×2 unit matrix. $\mathbf{L}^n$ with an odd index n can be found from

$$\mathbf{L}^{2j-1} = \mathcal{L}^{j-1}\mathbf{L}, \quad j = 1, 2, \ldots, \tag{12}$$

and $\mathbf{L}^n$ with an even index n is

$$\mathbf{L}^{2j} = \mathcal{L}^j\mathbf{I}, \quad j = 1, 2, \ldots. \tag{13}$$

From (10) and (11), we can represent the discrete time solutions of (6) with a given accuracy in a recursive manner as

$$\begin{pmatrix} u_{n+1} \\ v_{n+1} \end{pmatrix} = \begin{pmatrix} I + \delta t^2\mathcal{L}/2 & \delta t + \delta t^3\mathcal{L}/6 \\ \delta t\mathcal{L} + \delta t^3\mathcal{L}^2/6 & I + \delta t^2\mathcal{L}/2 \end{pmatrix}\begin{pmatrix} u_n \\ v_n \end{pmatrix} + \mathcal{O}(\delta t^4), \tag{14}$$

or

$$\begin{pmatrix} u_{n+1} \\ v_{n+1} \end{pmatrix} = \begin{pmatrix} I + \delta t^2\mathcal{L}/2 & \delta t \\ \delta t\mathcal{L} & I + \delta t^2\mathcal{L}/2 \end{pmatrix}\begin{pmatrix} u_n \\ v_n \end{pmatrix} + \mathcal{O}(\delta t^3). \tag{15}$$

The operator matrix $\mathbf{L}$ in a system of first-order differential equations (8) can be represented by eigenvalues (λ_j) and eigenvectors (y_j)

$$\mathbf{L}y_j = \lambda_j y_j, \quad j = 1, 2. \tag{16}$$

The eigenvalues λ_j $(j = 1, 2)$ of the matrix $\mathbf{L}$ are given by

$$\lambda_1 = c\partial_x, \quad \lambda_2 = -c\partial_x, \tag{17}$$

where c is the wave speed.

The stability and stiffness of the equation system (8) are related to the eigenvalues λ_j ($j = 1, 2$) of the operator matrix $\mathbf{L}$. For stability, $\lambda_j \leq 1$. Note that a system of first-order differential equations is stiff if at least one eigenvalue has a large negative real part, which causes the corresponding component of the solution to vary rapidly compared to the typical scale of variation displayed by the rest of the solution (see [32]). The stiffness ratio R_s of an operator matrix $\mathbf{L}$ is given by

$$R_s = \frac{Max|\lambda_j|}{Min|\lambda_j|} = \frac{|c\partial_x|}{|-c\partial_x|} = 1, \tag{18}$$

where $j = 1, 2$. As the stiffness ratio is equal to 1, this system of coupled linear differential equations is not stiff. But for numerical stability during modelling, a time step size δt must satisfy the condition (see [24])

$$\delta t < \frac{K_a}{Max|\lambda_j|} = \frac{K_a}{c|\partial_x|}, \tag{19}$$

where K_a is a constant dependent on the method chosen. Since the operator ∂_x is represented in the form of a matrix (i.e., a matrix operator) in the physical domain, $|\partial_x|$ corresponds to the determinant of the matrix operator. The magnitude of the determinant becomes larger as the grid step (δx) becomes smaller. In other words, the more samples in space are used in the analysis, the smaller time step δt is needed.

4.2. Application of the Numerical Method

In this section, we consider a boundary value problem for acoustic waves. Such boundary value problems are commonly met in natural problems and only a few cases can be solved analytically. We consider a string which is constrained at both ends with specified initial conditions. In this case the pulse propagates backward with a reversed phase when it meets an end of the string. The boundary conditions are given by

$$u(x_s, t) = 0, \quad u(x_e, t) = 0, \tag{20}$$

where x_s is set to be 0 and x_e be 1. We apply a discrete scheme to the governing equations, implementing (14) with fourth-order accuracy. The boundary conditions at both ends of the string are considered through several different approaches. Then we compare the performance of the schemes by the level of agreement of the results with analytic solutions, expressed using a Fourier basis (see [60]).

We introduce three different ways to implement boundary conditions: by direct application to a grid point, by direct application on a band of gird points, and via equivalent forces. In principle, one can satisfy the boundary conditions at both end of string by considering those at just one end since the wavelet-based method incorporates a periodic boundary condition inherently. To implement the boundary conditions via additional equivalent force terms in a semigroup approach, we rewrite the governing equations as

$$\partial_t \mathbf{U} = \mathbf{L}\mathbf{U} + \mathbf{N}, \tag{21}$$

where $\mathbf{U}$ is a vector unknown composed of the displacement and velocity (u, v), $\mathbf{L}$ is the

operator matrix given in (9), and the vector for the equivalent force terms $\mathbf{N}$ is

$$\mathbf{N} = \left\{ \sum_{i=1}^{n_b} \delta(x - x_i) \right\} \cdot \begin{pmatrix} -v \\ -\mathcal{L}u \end{pmatrix}, \tag{22}$$

where n_b is the number of grid points at which boundary conditions are applied and x_i the corresponding positions. Using the semigroup approach, the general solution $\mathbf{U}(x, t)$ of the first-order PDE system (21) is given by

$$\mathbf{U}(x, t) = e^{t\mathbf{L}}\mathbf{U}(x, 0) + \int_0^t e^{\mathbf{L}(t-\tau)}\mathbf{N}(x, \tau)\, d\tau, \tag{23}$$

where $\mathbf{U}(x, 0)$ is an initial condition. Therefore, following (5), we can obtain the discrete time solution for the general solution (23) as

$$\mathbf{U}_{n+1} = e^{\delta t\mathbf{L}}\mathbf{U}_n + \delta t(\gamma\mathbf{N}_{n+1} + \beta_0\mathbf{N}_n), \tag{24}$$

where $\mathbf{U}_n$ is a vector unknown and $\mathbf{N}_n$ is a vector for equivalent force terms at a discretized time t_n. When $\gamma = 0$ (explicit case), β_0 is determined as $(e^{\delta t\mathbf{L}} - \mathbf{I})(\delta t\mathbf{L})^{-1}$ and this can be approximated by a Taylor expansion:

$$\beta_0 = \mathbf{I} + \frac{1}{2}\delta t\mathbf{L} + \frac{1}{6}\delta t^2\mathbf{L}^2 + \frac{1}{24}\delta t^3\mathbf{L}^3 + \cdots. \tag{25}$$

The resultant form of β_0 is

$$\beta_0 = -\left\{ \sum_{i=1}^{n_b} \delta(x - x_i) \right\} \cdot \begin{pmatrix} v + \delta t\mathcal{L}u/2 + \delta t^2\mathcal{L}v/6 + \delta t^3\mathcal{L}^2u/24 \\ \mathcal{L}u + \delta t\mathcal{L}v/2 + \delta t^2\mathcal{L}^2u/6 + \delta t^3\mathcal{L}^2v/24 \end{pmatrix}. \tag{26}$$

4.3. Acoustic Wave Propagation

We consider an acoustic wave propagation in one space dimension using the scheme developed in Sections 4.1 and 4.2.

The domain is split into 128 grid points and the both ends of domain are considered as rigid boundaries. As a solution of the wave equation (6) takes the form $f(x - ct)$, we set the initial conditions as

$$f(x - ct) = e^{-300(x-0.5-ct)^2}, \quad 0 < x \le 1, \tag{27}$$

and then initial conditions $u_0(x)$ and $v_0(x)$ are $f(x - ct)$ and $-cf'(x - ct)$ at $t = 0$ (Fig. 3). In this application we set a wave speed c to be 0.302.

We attempt to satisfy a rigid boundary condition at both ends using three different approaches and compare the results with analytic solutions. The first approach is to set displacement and velocity at one end of string to be zero (namely, $u(1) = v(1) = 0$) directly in computation procedure. The second is to introduce the artificial extension of boundaries of the domain (i.e., $0 < x \le 1 + b_w$) where b_w is a band width corresponding to a rigid strip, and then displacement and velocity at the region are set to be null (i.e., $u(x_j) = v(x_j) = 0$, $j = n, n + 1, \ldots, m$ where $x_n = 1$, $x_m = 1 + b_w$). The third is to implement equivalent force terms (22) explicitly at the artificial boundary region while applying a semigroup approach.

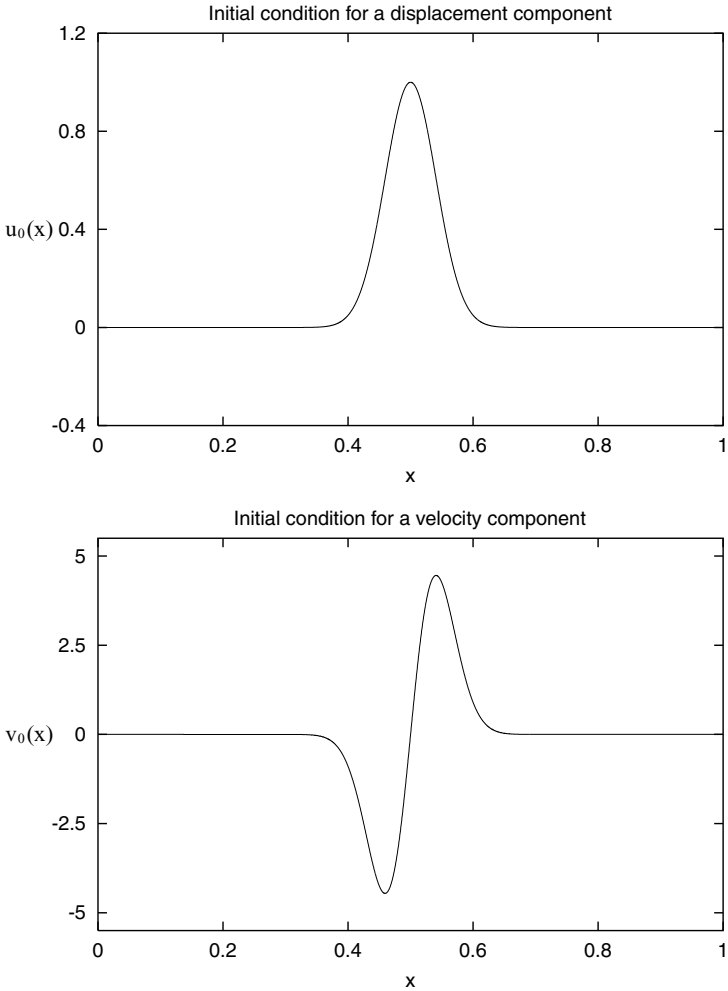

FIG. 3. Initial conditions for the displacement component, $u_0(x)$, and the velocity component, $v_0(x)$, for the numerical modelling of acoustic wave propagation in a 1-D space.

The analytic solutions $u(x, t)$ $(0 \leq x \leq l)$ of boundary value problem can be obtained using Fourier series as

$$u(x,t) = \sum_{n=1}^{\infty} \sin \lambda_n x \cdot (a_n \cos \lambda_n ct \; + \; b_n \sin \lambda_n ct), \tag{28}$$

where a_n, b_n is represented with initial values of displacement and velocity components $(u_0(x), v_0(x))$:

$$\begin{aligned} a_n &= \frac{2}{l} \int_0^l u_0(x) \sin\left(\frac{n\pi x}{l}\right) dx, \\ b_n &= \frac{2}{n\pi c} \int_0^l v_0(x) \sin\left(\frac{n\pi x}{l}\right) dx. \end{aligned} \tag{29}$$

l is the length of the domain and $\lambda_n = n\pi/l$. In this case, l is 1.

Figure 4 shows comparisons between the numerical results and analytic solutions at time $t = 1, 6, 29$ s. When the boundary condition is considered at just a single grid point of the

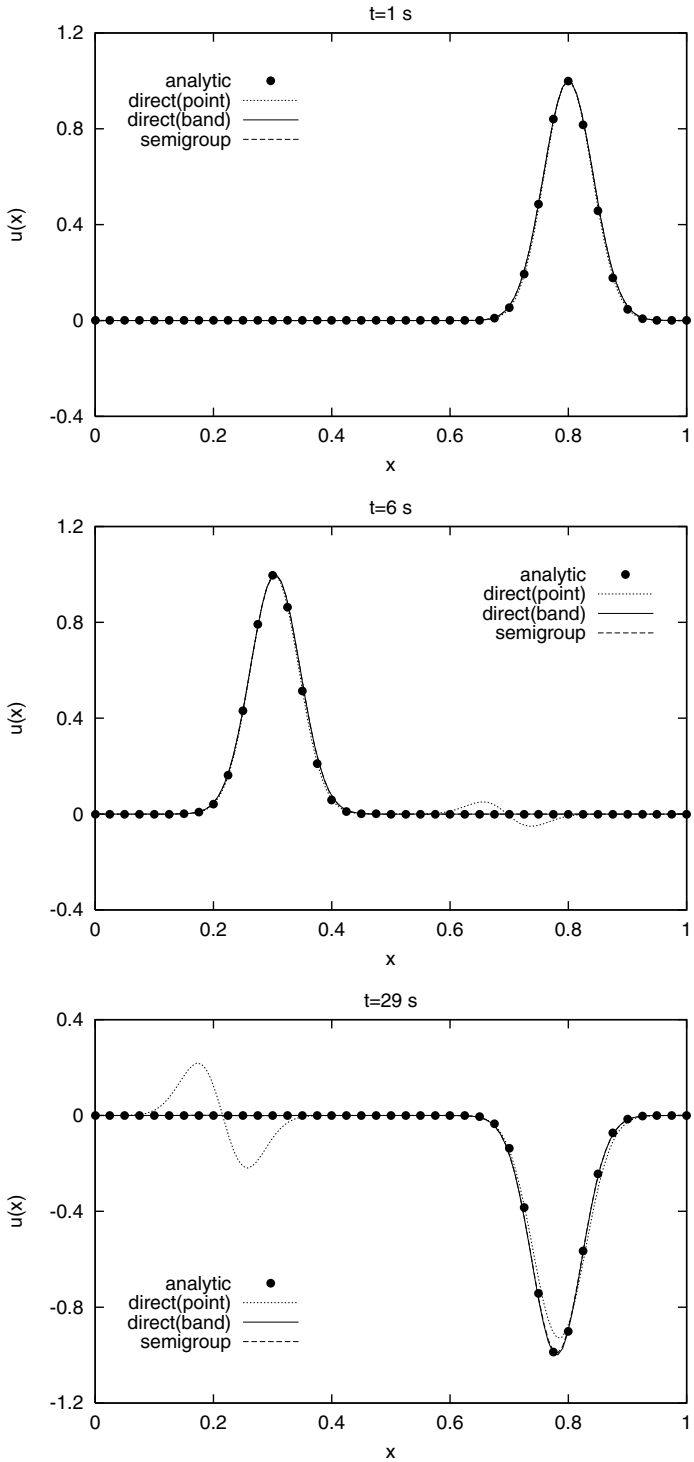

FIG. 4. Comparison among various numerical results with analytic solutions for the acoustic wave propagation in a 1-D space.

string, the energy in the waves leaks and the amplitude of reflected main phase is gradually reduced, while the spurious waves from energy leakage become larger as the number of reflections on the boundaries increases. Physically, the modelled string corresponds to successive strings having their own initial conditions, which are connected at the constraint points in a chain due to inherent periodic boundary condition of the wavelet method. Therefore, this pointwise constraint can not represent properly the physical rigid boundary. The use of rigid strip (5 grid points in this study) in the other two cases can reproduce the physical boundary effects well by isolating the system satisfactorily and exhibits a good agreement with the analytic solution. The technique using equivalent forces for the treatment of the boundary conditions not only produces accurate numerical results, but also fits directly into semigroup scheme with consequent gains in simplicity of codes by dividing into a main procedure and force effects. Therefore, the technique can be used efficiently for problems with complex boundary conditions to be implemented during main computational procedure. We implement the technique using equivalent forces in elastic wave problems to treat traction-free boundary conditions on a free surface.

5. ELASTIC WAVE EQUATIONS

5.1. Numerical Formulation

We consider the elastic wave equations for two space dimensions, which include body force terms and boundary conditions with compounds of spatial derivative terms. The partial differential equations describing *P-SV* wave propagation in 2-D media are given by

$$\begin{aligned}\frac{\partial^2 u_x}{\partial t^2} &= \frac{1}{\rho}\left(\frac{\partial \sigma_{xx}}{\partial x} + \frac{\partial \sigma_{xz}}{\partial z} + f_x\right),\\ \frac{\partial^2 u_z}{\partial t^2} &= \frac{1}{\rho}\left(\frac{\partial \sigma_{xz}}{\partial x} + \frac{\partial \sigma_{zz}}{\partial z} + f_z\right),\end{aligned} \tag{30}$$

where (u_x, u_z) is the displacement vector and $(\sigma_{xx}, \sigma_{xz}, \sigma_{zz})$ are elements of the stress tensor. The stress components $\sigma_{xx}, \sigma_{xz}, \sigma_{zz}$ are expressed using compounds of spatial derivatives of displacement components as

$$\begin{aligned}\sigma_{xx} &= (\lambda + 2\mu)\frac{\partial u_x}{\partial x} + \lambda \frac{\partial u_z}{\partial z},\\ \sigma_{zz} &= \lambda \frac{\partial u_x}{\partial x} + (\lambda + 2\mu)\frac{\partial u_z}{\partial z},\\ \sigma_{xz} &= \mu\left(\frac{\partial u_x}{\partial z} + \frac{\partial u_z}{\partial x}\right),\end{aligned} \tag{31}$$

where $\lambda(x, z)$ and $\mu(x, z)$ are the Lamè coefficients.

The right-hand sides of Eq. (30) can be simplified by introducing linear operators $\mathcal{L}_{ij}$ $(i, j = x, z)$ of whose effects can be estimated in physical space by the representation of the operators on wavelet bases. The elastic wave equations in (30) are considered as

second-order differential equations in time,

$$\begin{aligned}\frac{\partial^2 u_x}{\partial t^2} &= \mathcal{L}_{xx}u_x + \mathcal{L}_{xz}u_z + \frac{f_x}{\rho},\\ \frac{\partial^2 u_z}{\partial t^2} &= \mathcal{L}_{zx}u_x + \mathcal{L}_{zz}u_z + \frac{f_z}{\rho},\end{aligned} \tag{32}$$

where the linear operators $\mathcal{L}_{ij}$ $(i, j = x, z)$ are

$$\begin{aligned}\mathcal{L}_{xx} &= \frac{1}{\rho}\frac{\partial}{\partial x}\left[(\lambda+2\mu)\frac{\partial}{\partial x}\right] + \frac{1}{\rho}\frac{\partial}{\partial z}\left[\mu\frac{\partial}{\partial z}\right],\\ \mathcal{L}_{xz} &= \frac{1}{\rho}\frac{\partial}{\partial x}\left[\lambda\frac{\partial}{\partial z}\right] + \frac{1}{\rho}\frac{\partial}{\partial z}\left[\mu\frac{\partial}{\partial x}\right],\\ \mathcal{L}_{zx} &= \frac{1}{\rho}\frac{\partial}{\partial x}\left[\mu\frac{\partial}{\partial z}\right] + \frac{1}{\rho}\frac{\partial}{\partial z}\left[\lambda\frac{\partial}{\partial x}\right],\\ \mathcal{L}_{zz} &= \frac{1}{\rho}\frac{\partial}{\partial x}\left[\mu\frac{\partial}{\partial x}\right] + \frac{1}{\rho}\frac{\partial}{\partial z}\left[(\lambda+2\mu)\frac{\partial}{\partial z}\right].\end{aligned} \tag{33}$$

To apply the semigroup approach to the elastic wave equations possibly to obtain the discrete time solutions, we rewrite (32) as a system of first-order differential equations by introducing additional unknowns for the velocity components. The resultant system of first-order PDEs for the displacement-velocity formulation is

$$\begin{aligned}\frac{\partial u_x}{\partial t} &= v_x,\\ \frac{\partial v_x}{\partial t} &= \mathcal{L}_{xx}u_x + \mathcal{L}_{xz}u_z + \frac{f_x}{\rho},\\ \frac{\partial u_z}{\partial t} &= v_z,\\ \frac{\partial v_z}{\partial t} &= \mathcal{L}_{zx}u_x + \mathcal{L}_{zz}u_z + \frac{f_z}{\rho},\end{aligned} \tag{34}$$

where v_j $(j = x, z)$ is the velocity component in j direction. Following the acoustic wave case, the system of equations in (34) can be written as a first-order differential equation with a vector unknown $\mathbf{U}$,

$$\partial_t \mathbf{U} = \mathbf{L}\mathbf{U} + \mathbf{F}, \tag{35}$$

where $\mathbf{U}$ is $(u_x, v_x, u_z, v_z)^{\mathrm{t}}$ and $\mathbf{F}$ is composed of directional forces as $(0, f_x/\rho, 0, f_z/\rho)^{\mathrm{t}}$. The operator matrix $\mathbf{L}$ is given by

$$\mathbf{L} = \begin{pmatrix} 0 & I & 0 & 0\\ \mathcal{L}_{xx} & 0 & \mathcal{L}_{xz} & 0\\ 0 & 0 & 0 & I\\ \mathcal{L}_{zx} & 0 & \mathcal{L}_{zz} & 0\end{pmatrix}. \tag{36}$$

5.2. Evaluation of Numerical Scheme

A system of first-order differential equations with body force terms in (34) cannot be applied directly to the numerical simulation of elastic wave propagation since the sudden application of a force generates instability around the source region. This phenomenon occurs due to multiple applications of derivative operators in the same direction on the delta function in the source region. To reduce the numerical instability, we introduce the source in a small region of locally homogeneous material embedded in an otherwise heterogeneous medium. We therefore assume that the physical parameters (λ, μ, ρ) are constant throughout the source region, with the result that the linear operators are simplified to the form $C_p \partial_i \partial_j$ $(i, j = x, z)$ where C_p are constants and a function of physical parameters. In the patch of uniform material, ∂_j^2 $(j = x, z)$ is obtained by the application of a second-order derivative operator rather than a double application of a first-order derivative operator.

The linear operators $\mathcal{L}_{ij}^h$ $(i, j = x, z)$ in a source region are given by

$$\mathcal{L}_{xx}^h = \frac{\lambda + 2\mu}{\rho}\frac{\partial^2}{\partial x^2} + \frac{\mu}{\rho}\frac{\partial^2}{\partial z^2}, \quad \mathcal{L}_{zz}^h = \frac{\mu}{\rho}\frac{\partial^2}{\partial x^2} + \frac{\lambda + 2\mu}{\rho}\frac{\partial^2}{\partial z^2},$$
$$\mathcal{L}_{xz}^h = \mathcal{L}_{zx}^h = \frac{\lambda + \mu}{\rho}\frac{\partial^2}{\partial x \partial z}, \tag{37}$$

where a superscript h is added for the simpler operators in the source region to distinguish from those in the main region. Therefore, the operator matrix $\mathbf{L}_h$ in this region is composed of $\mathcal{L}_{ij}^h$ (cf., (36)). Considering the general solution in (23), the discrete time solution is given by

$$\mathbf{U}_{n+1} = e^{\delta t \mathbf{L}_h}\mathbf{U}_n + \delta t \boldsymbol{\beta}_0 \mathbf{F}_n, \tag{38}$$

where δt is a time step and $\mathbf{F}_n$ is a force vector at a discretized time t_n. Following the scheme in acoustic wave case, $e^{\delta t \mathbf{L}_h}$ and $\boldsymbol{\beta}_0$ can be approximated by a Taylor expansion (cf. (11), (25)).

We consider the source-region scheme during body force activation and implement the heterogeneous-media scheme for the modelling of elastic wave propagation in the rest of the medium. As the body force only needs to be considered in the source region, we can omit the source term f_j $(j = x, z)$ in the governing equations (30) for the heterogeneous zone. Therefore, the system of first-order differential equation in the main region can be written as

$$\partial_t \mathbf{U} = \mathbf{L}\mathbf{U}, \tag{39}$$

where $\mathbf{L}$ is a 4-by-4 operator matrix and the components of $\mathbf{L}$, $\mathcal{L}_{ij}$ $(i, j = x, z)$ are given in (33). Using a semigroup approach and the discrete representation (5), Eq. (39) can be discretized as

$$\mathbf{U}_{n+1} = e^{\delta t \mathbf{L}}\mathbf{U}_n, \tag{40}$$

where again $e^{\delta t \mathbf{L}}$ is evaluated using a Taylor expansion as in (11).

5.3. Treatment of Boundary Conditions

One of difficulties in the numerical simulation of elastic wave propagation is the treatment of the boundary conditions. Two kinds of boundary conditions are usually needed: absorbing boundary conditions and traction-free boundary conditions. Absorbing boundary conditions are introduced to treat the artificial boundaries which are generated due to the confinement (artificial bounds) of the numerical domain. Traction-free boundary conditions are implemented to consider the effect of a free surface.

5.3.1. *Absorbing Boundary Conditions*

In a numerical modelling, the occurrence of artificial boundaries is an inevitable limitation. We note that many numerical studies based on wavelets have considered special cases when periodic boundary conditions are applied at those artificial boundaries (e.g., [9]). However, for studies of physical transient phenomenon, especially modelling of elastic wave propagation, it is important to design good absorbing boundaries to reduce spurious phenomena. Historically, many studies have concentrated theoretically and technically on development of satisfactory absorbing boundary conditions in numerical modelling history (e.g., [17, 19, 29, 48, 66, 67, 78]). However, the explicit implementation of absorbing boundary conditions sometimes can evoke an instability in modelling and result in numerical dispersion (see [54]) and the absorption rate of waves can be dependent on the incident angle of waves to a boundary (see [17]). Moreover, the explicit implementation of absorbing boundary conditions needs additional numerical work on the boundaries with a consequent time cost.

To treat absorbing boundaries in a consistent way, we consider the boundary conditions in the equation system implicitly, by including additional attenuation terms which make energy of incoming waves dissipated during propagation in the absorbing regions (see [48, 67]). For this purpose, we make attenuation active around the artificial boundaries by assigning non-zero attenuation terms around the boundaries and zero in the main computational domain. The attenuation terms are designed to be bounded, twice differentiable (see spatial operators $\mathcal{L}_{ij}$) and to have a sufficiently smooth derivative in order to make amplitudes of waves incident on the boundaries reduce gradually and continuously without generation of spurious waves reflected from the attenuation gradient (see [67]).

When we introduce attenuation factors (Q_x, Q_z) into the elastic wave equations, we add an extra first-order time derivative term (e.g., $2Q_x\partial_t u_x$) in governing equation system (30) (cf. [67]). The governing equation system with attenuation terms can be then written as

$$\begin{aligned}
\frac{\partial^2 u_x}{\partial t^2} + 2Q_x\frac{\partial u_x}{\partial t} &= \frac{1}{\rho}\left(\frac{\partial \sigma_{xx}}{\partial x} + \frac{\partial \sigma_{xz}}{\partial z}\right),\\
\frac{\partial^2 u_z}{\partial t^2} + 2Q_z\frac{\partial u_z}{\partial t} &= \frac{1}{\rho}\left(\frac{\partial \sigma_{xz}}{\partial x} + \frac{\partial \sigma_{zz}}{\partial z}\right).
\end{aligned} \tag{41}$$

In this case, the operator matrix $\mathbf{L}_q$ becomes

$$\mathbf{L}_q = \begin{pmatrix} 0 & I & 0 & 0\\ \mathcal{L}_{xx} & -2Q_x & \mathcal{L}_{xz} & 0\\ 0 & 0 & 0 & I\\ \mathcal{L}_{zx} & 0 & \mathcal{L}_{zz} & -2Q_z \end{pmatrix}. \tag{42}$$

Following (40) and evaluating $e^{\delta t \mathbf{L}_q}$ by a Taylor expansion, we discretize the first-order differential equation system and the discretized solution of (41) is given by

$$\mathbf{U}_{n+1} = \mathbf{U}_n + \delta t\, \mathbf{L}_q \mathbf{U}_n + \frac{1}{2}\delta t^2\, \mathbf{L}_q^2 \mathbf{U}_n + \cdots + \frac{1}{m!}\delta t^m\, \mathbf{L}_q^m \mathbf{U}_n + \mathcal{O}(\delta t^{m+1}). \tag{43}$$

The relationship between the time step (δt) and a truncation order (m) implemented in discrete time solution (43) is considered in Section 5.6, and the parameters for attenuation terms are considered in Section 6.1. We refer to the previous work of the authors [34] for the quantitative analysis of spurious waves generation from artificial boundaries in the implementation of these absorbing boundary conditions.

5.3.2. *Traction-Free Boundary Conditions*

Following the explicit implementation procedure of boundary conditions as in acoustic wave problems, the traction-free boundary conditions are considered via introduction of equivalent force terms.

For a flat free surface normal to the z-axis the traction-free boundary condition in two space dimensions requires the vanishing of normal and tangential tractions at the free surface ($z = 0$):

$$[\sigma_{iz}]_{z=0} = 0, \quad i = x, z. \tag{44}$$

Since the explicit form of condition is given to 'only' traction terms (σ_{xz}, σ_{zz}), the other variables (e.g., σ_{xx}) on the boundary need to be updated at each discrete time considering the variation of the tractions (cf. [30, 72]). For this purpose, finite difference methods assign values to displacement terms in an artificially extended region over the free surface boundary so that tractions on the boundary can be forced to vanish. In addition, the procedure for a numerical differentiation is modified at the free surface to make the other variables balanced during implementation of the boundary conditions [31, 58, 77]. An alternative technique using the one-dimensional analysis scheme based on characteristic variables which sets outgoing characteristic variables equal to those expected by numerical scheme when the traction-free condition is satisfied has been implemented in Chebychev-pseudospectral methods (e.g., [15, 47, 70]) and in the finite difference method (e.g., [4]).

With the introduction of the displacement-velocity formulation, which does not assign stress terms as variables explicitly during the computation, we can implement the free surface effects through consideration of the stress variations on the boundary via equivalent forces. The tractions are forced to zero but we also need to determine the behaviour of σ_{xx}. Since there is a displacement discontinuity over the free surface, the vertical spatial differentiation in σ_{xx} (i.e., $\partial_z u_z$) is replaced through use of the boundary condition, $\sigma_{zz} = 0$. Thus using the expression for $\sigma_{zz} = 0$, the vertical derivative term can be represented by the horizontal derivative term on a free surface:

$$\frac{\partial u_z}{\partial z} = -\frac{\lambda}{\lambda + 2\mu}\frac{\partial u_x}{\partial x}. \tag{45}$$

From (45), σ_{xx} at the free surface can be expressed as

$$\sigma_{xx}|_{z=0} = \frac{4\mu(\lambda + \mu)}{(\lambda + 2\mu)}\frac{\partial u_x}{\partial x}. \tag{46}$$

Note that the expression (46) is the same expression as that produced by the one-dimensional analysis technique (see [15]). Now, the governing equations including both absorbing and traction-free boundary conditions can be written as

$$\begin{aligned}\frac{\partial^2 u_x}{\partial t^2} &= -2Q_x\frac{\partial u_x}{\partial t} + \frac{1}{\rho}\left\{\frac{\partial}{\partial x}\left(\sigma_{xx} - \sigma_{xx}^F + \sigma_{xx}^M\right) + \frac{\partial}{\partial z}\left(\sigma_{xz} - \sigma_{xz}^F\right) + f_x\right\},\\ \frac{\partial^2 u_z}{\partial t^2} &= -2Q_z\frac{\partial u_z}{\partial t} + \frac{1}{\rho}\left\{\frac{\partial}{\partial x}\left(\sigma_{xz} - \sigma_{xz}^F\right) + \frac{\partial}{\partial z}\left(\sigma_{zz} - \sigma_{zz}^F\right) + f_z\right\},\end{aligned} \tag{47}$$

where

$$\begin{aligned}\sigma_{ij}^F &= \delta(z)\sigma_{ij}, \quad i, j = x, z,\\ \sigma_{xx}^M &= \delta(z)\left\{\frac{4\mu(\lambda+\mu)}{(\lambda+2\mu)}\frac{\partial u_x}{\partial x}\right\}.\end{aligned} \tag{48}$$

The equivalent force terms for traction-free conditions can be considered via forcing terms, and thereby the equation system with a displacement-velocity formulation can be expressed by

$$\partial_t \mathbf{U} = \mathbf{L}_q\mathbf{U} + \mathbf{N}, \tag{49}$$

where $\mathbf{N}$ is a vector for body forces and equivalent force terms expressing traction-free boundary conditions and operator matrix $\mathbf{L}_q$ includes the absorbing boundary conditions. The vector $\mathbf{N}$ is composed of four equivalent force terms ($\mathcal{N}(v_j), \mathcal{N}(u_j)$, $j = x, z$):

$$\begin{aligned}\mathcal{N}(u_x) &= \mathcal{N}(u_z) = 0,\\ \mathcal{N}(v_x) &= \frac{1}{\rho}\left\{f_x - \frac{\partial\sigma_{xx}^F}{\partial x} - \frac{\partial\sigma_{xz}^F}{\partial z} + \frac{\partial\sigma_{xx}^M}{\partial x}\right\},\\ \mathcal{N}(v_z) &= \frac{1}{\rho}\left\{f_z - \frac{\partial\sigma_{xz}^F}{\partial x} - \frac{\partial\sigma_{zz}^F}{\partial z}\right\}.\end{aligned} \tag{50}$$

In an approach comparable to the implementation of boundary conditions in acoustic wave problems in Section 4.3, we introduce a zero-velocity artificial layer ($\lambda = \mu = 0$) above the free surface. This has the effect of confining the elastic wave in the domain to which equivalent forces are applied on the boundary, and significantly improves the accuracy.

Finally, considering (38), (11), and (43), we can express the discrete time solution for the elastic wave equation including implicitly absorbing and traction-free conditions as

$$\begin{aligned}\mathbf{U}_{n+1} = \mathbf{U}_n &+ \delta t\,\mathbf{L}_q\mathbf{U}_n + \frac{\delta t^2}{2}\mathbf{L}_q^2\mathbf{U}_n + \cdots + \frac{\delta t^m}{m!}\mathbf{L}_q^m\mathbf{U}_n\\ &+ \delta t\,\mathbf{N}_n + \frac{\delta t^2}{2}\mathbf{L}_q\mathbf{N}_n + \frac{\delta t^3}{6}\mathbf{L}_q^2\mathbf{N}_n + \cdots + \frac{\delta t^{m+1}}{(m+1)!}\mathbf{L}_q^m\mathbf{N}_n,\end{aligned} \tag{51}$$

where $\mathbf{U}_n$ is a variable vector at discrete time t_n and $\mathbf{N}_n$ is a vector for forcing terms.

5.4. Introduction of a Grid Generation Scheme

To treat a medium with topography in the wavelet-based method, we introduce a grid generation technique (or grid-mapping technique) [70]; a rectangular grid system can be

mapped into a curved grid system considering physical topography by using an one dimensional linear stretch in the vertical direction. For convenience, we set the topography of the bottom artificial boundary to be same as that of the free surface and stretch the grids from the free surface to the lower artificial boundary. So, the function of grid mapping from a ξ-η coordinate system to a x-z coordinate system is given by

$$\begin{aligned} x(\xi, \eta) &= \xi, \\ z(\xi, \eta) &= z_0(\xi) + \eta, \end{aligned} \tag{52}$$

where $z_0(\xi)$ is a topography of a free surface which depends on only ξ, and the rectangular domain size is considered to be normalized so as to satisfy $0 < \xi, \eta \leq 1$.

The spatial derivatives of any variable g in a physical grid system can be represented using a chain rule by

$$\begin{aligned} \frac{\partial g}{\partial x} &= \frac{\partial \xi}{\partial x}\frac{\partial g}{\partial \xi} + \frac{\partial \eta}{\partial x}\frac{\partial g}{\partial \eta}, \\ \frac{\partial g}{\partial z} &= \frac{\partial \xi}{\partial z}\frac{\partial g}{\partial \xi} + \frac{\partial \eta}{\partial z}\frac{\partial g}{\partial \eta}, \end{aligned} \tag{53}$$

where the matrices of the transformation are given by

$$\begin{aligned} \frac{\partial \xi}{\partial x} &= J\frac{\partial z}{\partial \eta}, \quad \frac{\partial \xi}{\partial z} = -J\frac{\partial x}{\partial \eta}, \\ \frac{\partial \eta}{\partial x} &= -J\frac{\partial z}{\partial \xi}, \quad \frac{\partial \eta}{\partial z} = J\frac{\partial x}{\partial \xi}, \end{aligned} \tag{54}$$

and the Jacobian J is

$$J = 1 \Big/ \left(\frac{\partial x}{\partial \xi}\frac{\partial z}{\partial \eta} - \frac{\partial x}{\partial \eta}\frac{\partial z}{\partial \xi} \right) = 1. \tag{55}$$

Therefore, from (54) and (55), Eq. (53) can be rewritten as

$$\begin{aligned} \frac{\partial g}{\partial x} &= \frac{\partial g}{\partial \xi} - \frac{\partial z_0}{\partial \xi}\frac{\partial g}{\partial \eta}, \\ \frac{\partial g}{\partial z} &= \frac{\partial g}{\partial \eta}. \end{aligned} \tag{56}$$

Using (56), we can rewrite the linear operator ($\mathcal{L}_{ij}, i, j = x, z$) for elastic wave equations in (33) with the remapped coordinate scheme

$$\begin{aligned} \mathcal{L}_{xx} &= \frac{1}{\rho}\left[\frac{\partial}{\partial \xi} - \frac{\partial z_0}{\partial \xi}\frac{\partial}{\partial \eta}\right]\left[(\lambda + 2\mu)\frac{\partial}{\partial \xi} - (\lambda + 2\mu)\frac{\partial z_0}{\partial \xi}\frac{\partial}{\partial \eta}\right] + \frac{1}{\rho}\frac{\partial}{\partial \eta}\left[\mu\frac{\partial}{\partial \eta}\right], \\ \mathcal{L}_{xz} &= \frac{1}{\rho}\frac{\partial}{\partial \eta}\left[\mu\frac{\partial}{\partial \xi} - \mu\frac{\partial z_0}{\partial \xi}\frac{\partial}{\partial \eta}\right] + \frac{1}{\rho}\left[\frac{\partial}{\partial \xi} - \frac{\partial z_0}{\partial \xi}\frac{\partial}{\partial \eta}\right]\left[\lambda\frac{\partial}{\partial \eta}\right], \\ \mathcal{L}_{zx} &= \frac{1}{\rho}\frac{\partial}{\partial \eta}\left[\lambda\frac{\partial}{\partial \xi} - \lambda\frac{\partial z_0}{\partial \xi}\frac{\partial}{\partial \eta}\right] + \frac{1}{\rho}\left[\frac{\partial}{\partial \xi} - \frac{\partial z_0}{\partial \xi}\frac{\partial}{\partial \eta}\right]\left[\mu\frac{\partial}{\partial \eta}\right], \\ \mathcal{L}_{zz} &= \frac{1}{\rho}\left[\frac{\partial}{\partial \xi} - \frac{\partial z_0}{\partial \xi}\frac{\partial}{\partial \eta}\right]\left[\mu\frac{\partial}{\partial \xi} - \mu\frac{\partial z_0}{\partial \xi}\frac{\partial}{\partial \eta}\right] + \frac{1}{\rho}\frac{\partial}{\partial \eta}\left[(\lambda + 2\mu)\frac{\partial}{\partial \eta}\right]. \end{aligned} \tag{57}$$

For numerical stability, we continue to use a locally homogeneous medium around the source. Following the scheme in Section 5.2, we assume physical parameters (λ, μ, ρ) are constant in the source region and therefore the linear operators $\mathcal{L}^h_{ij}$ $(i, j = x, z)$ for the source region can be written as

$$\begin{aligned}
\mathcal{L}^h_{xx} &= \frac{\lambda+2\mu}{\rho}\frac{\partial^2}{\partial\xi^2} - \frac{\lambda+2\mu}{\rho}\frac{\partial^2 z_0}{\partial\xi^2}\frac{\partial}{\partial\eta} - \frac{2(\lambda+2\mu)}{\rho}\frac{\partial z_0}{\partial\xi}\frac{\partial^2}{\partial\xi\,\partial\eta} \\
&\quad + \left[\frac{\lambda+2\mu}{\rho}\left(\frac{\partial z_0}{\partial\xi}\right)^2 + \frac{\mu}{\rho}\right]\frac{\partial^2}{\partial\eta^2}, \\
\mathcal{L}^h_{xz} &= \mathcal{L}^h_{zx} = \frac{(\lambda+\mu)}{\rho}\frac{\partial^2}{\partial\xi\,\partial\eta} - \frac{\lambda+\mu}{\rho}\frac{\partial z_0}{\partial\xi}\frac{\partial^2}{\partial\eta^2}, \\
\mathcal{L}^h_{zz} &= \frac{\mu}{\rho}\frac{\partial^2}{\partial\xi^2} - \frac{\mu}{\rho}\frac{\partial^2 z_0}{\partial\xi^2}\frac{\partial}{\partial\eta} - \frac{2\mu}{\rho}\frac{\partial z_0}{\partial\xi}\frac{\partial^2}{\partial\xi\,\partial\eta} + \left[\frac{\mu}{\rho}\left(\frac{\partial z_0}{\partial\xi}\right)^2 + \frac{\lambda+2\mu}{\rho}\right]\frac{\partial^2}{\partial\eta^2}.
\end{aligned} \tag{58}$$

To satisfy the traction-free boundary conditions on a free surface in a medium with topography, we consider stress terms on a rotated local coordinate system (x', z') where the z' axis is perpendicular and the x' axis is parallel to the tangent to the free surface. The angle of rotation (θ) is determined by the rate of variation of local topography compared to the horizontal distance (ξ) in the rectangular grid system,

$$\theta = \tan^{-1}\left(\frac{\partial z_0(\xi)}{\partial\xi}\right), \tag{59}$$

where $z_0(\xi)$ is the topography of the surface as a function of horizontal position (ξ).

The relationships among the stress components in the physical coordinate system and a rotated local coordinate system are given by (see [70])

$$\sigma_{ij} = \sum_m \sum_n a_{mi} a_{nj} \sigma'_{mn}, \tag{60}$$

and

$$\sigma'_{ij} = \sum_m \sum_n a_{im} a_{jn} \sigma_{mn}, \tag{61}$$

where $i, j, m, n = x, z$ and the directional cosines are

$$\begin{pmatrix} a_{xx} & a_{xz} \\ a_{zx} & a_{zz} \end{pmatrix} = \begin{pmatrix} \cos\theta & \sin\theta \\ -\sin\theta & \cos\theta \end{pmatrix}. \tag{62}$$

From (60), we can estimate σ'_{mn} using σ_{ij}. As σ'_{xz} and σ'_{zz} are zero on the free surface, we can write equivalent force terms for a free surface boundary using σ_{jz} $(j = x, z)$ in the form

$$\begin{aligned}
\mathcal{N}(u_x) &= \mathcal{N}(u_z) = 0, \\
\mathcal{N}(v_x) &= \frac{1}{\rho}\left\{ f_x - \frac{\partial}{\partial x}\Sigma^F_{xx} - \frac{\partial}{\partial z}\Sigma^F_{xz} \right\}, \\
\mathcal{N}(v_z) &= \frac{1}{\rho}\left\{ f_z - \frac{\partial}{\partial x}\Sigma^F_{xz} - \frac{\partial}{\partial z}\Sigma^F_{zz} \right\},
\end{aligned} \tag{63}$$

where Σ_{ij}^F $(i, j = x, z)$ is the composite effects of the stress components at the free surface which can be computed from (50) and (60) by

$$\begin{aligned}
\Sigma_{xx}^F &= \delta(z)\left(\sigma_{xx} - \cos^2\theta\ \sigma'^M_{xx}\right),\\
\Sigma_{xz}^F &= \delta(z)\left(\sigma_{xz} - \sin\theta\cos\theta\ \sigma'^M_{xx}\right),\\
\Sigma_{zz}^F &= \delta(z)\left(\sigma_{zz} - \sin^2\theta\ \sigma'^M_{xx}\right).
\end{aligned} \tag{64}$$

Here, σ'^M_{xx} is a corrected stress term (see, Section 5.3.2) for σ'_{xx} at a free surface in a rotated local coordinate system including the effect of topography

$$\sigma'^M_{xx} = \frac{(\lambda + 2\mu)\sigma'_{xx} - \lambda\sigma'_{zz}}{\lambda + 2\mu}, \tag{65}$$

where the stress components σ'_{jz} $(j = x, z)$ on the free surface can be computed from (61).

5.5. Computational Steps

We describe the computational steps to implement the wavelet-based method for a modelling of elastic wave propagation.

Step 1: Assign physical parameters (e.g., λ, μ, ρ) at domain.
Step 2: Initialize variables (e.g., u_x, u_z, v_x, v_z) following initial conditions.
Step 3: Compute matrix operators for spatial derivatives in each direction (e.g., ∂_x, ∂_z).
Step 4: Start of time stepping.
Step 4.1: Compute operated variables (e.g., $\mathbf{L}^m\mathbf{U}_n$) using operator matrix.
Step 4.2: Compute effects of forcing terms including body force terms and traction-free boundary condition.
Step 4.3: Update the variables for t_{n+1} (e.g., $\mathbf{U}_{n+1}$).
Step 4.4: Iterate from 4.1 to 4.3 up to a given truncation order.
Step 5: Record numerical responses at specific receivers.
Step 6: Iterate Step 4 up to a given time.
Step 7: End of computation.

5.6. Stability and Numerical Analysis

For stable computation in numerical modelling, one has to consider two kinds of conditions: the time step condition and the grid dispersion condition. The usual time step (δt) condition for grid steps $(\delta x, \delta z)$ in grid-based methods for 2-D elastic waves is independent of the S wave velocity or of the Poisson's ratio ν, but related with largest wave speed (usually P wave velocity, α) of a domain. We set δx to be equal to δz in this study. Then an empirical stability condition for the relationship between the time step and the grid step (cf. [75]) can be expressed as

$$K_e\,\alpha_{max}\,\frac{\delta t}{\delta z} < 1, \tag{66}$$

where α_{max} is the highest wave velocity in the domain and K_e is a constant depending on the maximum order (m) of term (i.e., truncation order) considered in a discrete time solution

(51) based on Taylor expansion. Empirically, the K_e value linearly decreases with increase in the truncation order; when $m = 2$, $K_e = 10$, when $m = 10$ $K_e = 2$, and when $m = 20$, $K_e = 1$. Since K_e is in inverse proportion to m, the total computational time is almost constant regardless of variation of m implemented. Also, since m (or K_e) is related only to the time step (δt), not to the grid sizes (δx, δz), the numerical accuracy of the wavelet-based method is held constant during computation. However, we found that effects from boundary forcing terms (e.g., traction-free boundary conditions) can be implemented more accurately with larger time step (i.e., larger values of m). Taking into account the representation of the physical medium, the frequency content of the source time function for suitable excitation, and the accuracy of modelling, we implement $m = 20$ for the maximum order of term considered (i.e., $K_e = 1$) in this study.

In numerical modelling of wave propagation, every numerical method needs to satisfy a minimum grid occupancy per wavelength not to evoke numerical grid dispersion. The grid dispersion condition is related to the slowest velocity (i.e., smallest wavelength) of elastic waves in a given medium (e.g., Rayleigh waves in a homogeneous medium with a free surface). Generally, the minimum number of grid points per wavelength varies with the type of wavelets implemented. From numerical experiments using Daubechies wavelets, a high-order wavelet (i.e., wavelets with large vanishing moments) needs much a smaller number of grid points per wavelength for stable computation than a low-order wavelet (i.e., wavelets with small vanishing moments); as the order of wavelets increases by a factor of 2, only half as many grid points are needed. Empirically, Daubechies-3 wavelets need 32 grid points, Daubechies-6 wavelets 16 grid points, and Daubechies-20 wavelets 3 grid points. However, it is rather difficult to obtain accurate Daubechies wavelet coefficients with high order using known numerical schemes (e.g., [65, 69]); due to instability and round-off error in numerical computation, the relationship between an order of wavelets and a minimum grid number cannot be carried indefinitely. In this study, Daubechies-6 wavelets (Fig. 1a) have been implemented for modelling acoustic wave propagation and Daubechies-20 wavelets (Fig. 1b) are used for modelling elastic wave propagation.

To provide a reasonable comparison with other numerical techniques (e.g., finite difference method), we consider the computational resources needed for a specific situation. We consider a medium with size 10-by-10 km, where the P wave velocity is 3.5 km/s, the S wave velocity 2.0 km/s, and the density 2.2 g/cm^3, with a line source which generates waves with dominant frequency 4.5 Hz. The fourth-order finite difference method (FDM) then needs 250-by-250 grid points and the wavelet-based method (WBM) based on Daubechies-20 wavelets needs 64-by-64 grid points. The discrete time step (δt) is 0.006 s for the fourth-order FDM and 0.0446 s for the WBM when $m = 20$. The memory occupation is 3.8 megabytes for the FDM and 2.5 megabytes for the WBM when variables are held with double-precision accuracy. The CPU time for computation of the time response for a 1 s interval is 126 s in FDM and 252 s in WBM on an Ultra Sparc III (360 MHz). The most time-consuming procedure in the WBM is differentiation (i.e., application of differential operator to velocity or displacement field; see [7]), which will need further improvement to achieve fast implementation. A comparison of seismograms using the WBM and the FDM is presented in Fig. 6 and exhibits good matches between the very different methods.

In order to convey an idea of the accuracy of proposed method, the number of grid points per wavelength needed for stable and accurate modelling has been often considered (e.g., [45]). The fourth-order FDM needs at least 5 grid points per wavelength in simple media [50]. However, it has been reported that more grid points are needed in a model with strong

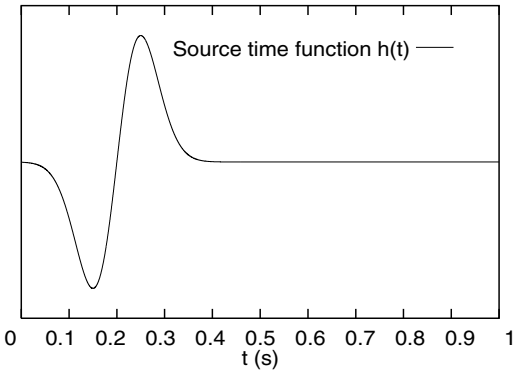

FIG. 5. Source time function $h(t)$ for the numerical modelling of elastic wave propagation.

impedance contrast between layers [64] such as the contact of liquid and solid layers. On the other hand, the WBM needs a constant number of grid points in any media (see also Section 6.3). For media with topography, the difference between the methods becomes larger and the WBM is more economical than the FDM. A FDM based on an unstructured grid system, which is suitable for topography problems, needs a dense grid system (about 20 grid points per wavelength; see [38]) for media with sinusoidal topography, while the WBM is still invariant (see Section 6.4.2).

This advantage of the WBM is particularly important for accurate modelling in random heterogeneous media or complex media, which have been considered for representation of heterogeneities in the crust, since quantitative estimates of wavefield properties are based on time responses from numerical modelling. In a recent study [35], we have shown that WBM generates accurate time responses in a random medium with very strong variation of physical parameters, while a fourth-order FDM displays artificially attenuated seismograms. Thus, the WBM can also be effective in Earth models, where wave velocities and physical

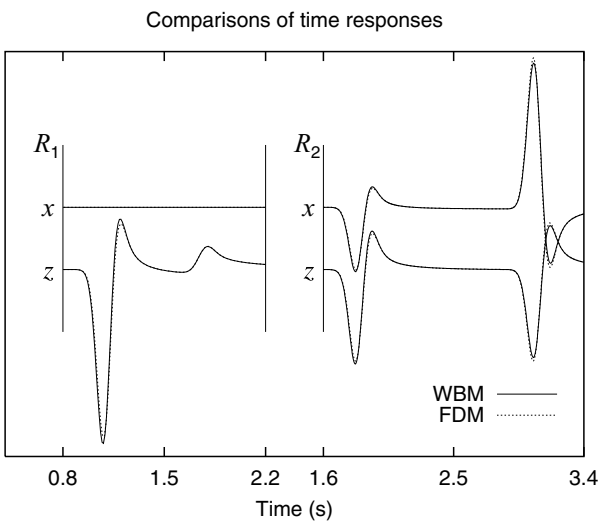

FIG. 6. Comparisons of time responses by a fourth-order finite difference method (FDM) and a wavelet-based method (WBM) in a homogeneous medium ($\alpha = 3.5$ km/s, $\beta = 2.0$ km/s, $\rho = 2.2$ g/cm^3). The receiver R_1 is located at (0 km, 3.125 km) from the source and R_2 is at (3.125 km, 3.125 km).

parameters are strongly dependent on depth, without the need for the introduction of a dense grid system.

For the stability test for the explicit implementation of traction-free boundary condition, we consider both high and low Poisson ratio cases ($\nu = 0.26, 0.4$) and compare numerical results with analytic solutions in Section 6.2.

6. NUMERICAL SIMULATIONS OF ELASTIC WAVE PROPAGATION

We apply the wavelet-based method to the modelling of elastic wave propagation and verify the results of the calculations with cases where analytic solutions are available and then extend to complex cases where no direct comparators are available. We consider homogeneous media with a flat surface or with a surface topography, layered heterogeneous media, and a stochastic heterogeneous medium with a fluid-filled crack.

6.1. Source and Initial Conditions

The sources are either a compressional point force or a vertically directed point force with a source time function $h(t)$ given by

$$h(t) = C_s(t - t_0)e^{-w(t-t_0)^2}, \tag{67}$$

where C_s is a constant value, t_0 is time shift, and w controls the wavelength content of the excitation. We set $t_0 = 0.2$ s and $w = 200$ (Fig. 5).

To construct suitable attenuation factors (Q_j, $j = x, z$) in (41) for numerical modelling, we follow the suggestions in [67]. We design Q_j to be bounded, twice differentiable and with a sufficiently smooth derivative. As the top boundary of a domain is considered a free surface, we distribute the attenuation terms so as not to disturb the effects from the presence of a free surface. Therefore, we shift the attenuation layers from top and bottom artificial boundaries by 20 material points to give

$$\begin{gathered} Q_j(i_x, i_z) = A_x\left[e^{B_x i_x^2} + e^{B_x(i_x - N_x)^2}\right] + A_z\left[e^{B_z(i_z+20)^2} + e^{B_z(i_z - N_z + 20)^2}\right], \\ j = x, z, \quad i_x = 1, 2, \ldots, N_x, \quad i_z = 1, 2, \ldots, N_z, \end{gathered} \tag{68}$$

where we use $A_x = A_z = 30$, $B_x = B_z = -0.015$, N_x is the number of grid points in the x direction, N_z the total number of grid points in the z direction and (i_x, i_z) is position in the discrete grid (Fig. 7). The initial condition is that the material is undistorted and at rest at time $t = 0$.

6.2. Homogeneous Media with a Planar Free Surface

First, we consider the excitation of elastic waves by a surface source in a homogeneous medium with a planar free surface (Lamb's problem). We check the stability and accuracy of the method with an explicit traction-free boundary condition by considering media with two different values of Poisson ratio ($\nu = 0.26$, 0.4). Since Earth materials generally have Poisson ratios between 0.22 and 0.35 (see [41, 42, 49]), the tests with two different Poisson ratios can justify the stability of the method for a general case. We note when $\nu = 0.5$, the medium would be fluid and then the governing equation can be written as an acoustic wave equation.

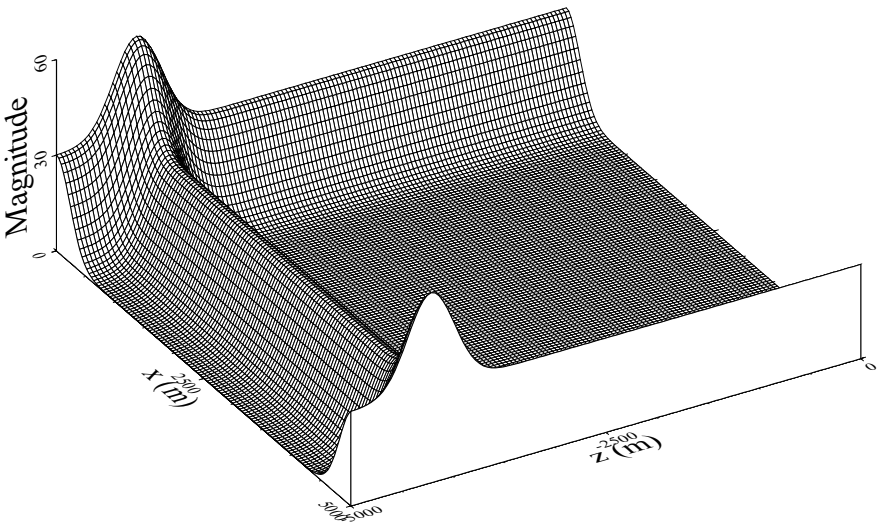

FIG. 7. The attenuation factor (Q_j, $j = x, z$) distribution on the 2-D media. To consider a top boundary as a free surface, the distribution of attenuation factors is shifted vertically by 20 rows of grids.

For the first experiment for Lamb's problem with $\nu = 0.26$, we consider the compressional wave speed α to be 3.5 km/s, the shear wave speed β to be 2.0 km/s, and the density ρ to be 2.2 g/cm^3 (see Fig. 8). Whereas for the second experiment with $\nu = 0.4$, the physical parameters of a medium are $\alpha = 4.4$ km/s, $\beta = 1.8$ km/s, and $\rho = 2.2$ g/cm^3. The $10\times$ 10 km^2 domain is represented through a 128×128 grid points.

The top boundary (Γ_T) is treated as a free surface where the traction vanishes, and the other three artificial boundaries (Γ_R, Γ_L, Γ_B) with absorbing boundary conditions following the technique in Sections 5.3.1 and 6.1. A vertically directed point force is applied at (3750 m, 2000 m). Figure 9 shows snapshots of elastic wave propagation for the two Poisson ratios.

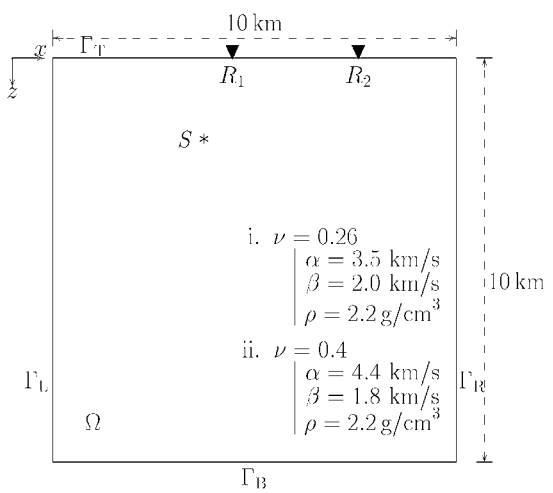

FIG. 8. Description of a homogeneous elastic medium with a planar free surface. Two different Poisson ratios ($\nu = 0.26, 0.4$) of physical parameters are considered for accuracy tests. S indicates a point source position and two receivers (R_1, R_2) are placed on the free surface at distances $x = 4453, 7578$ m.

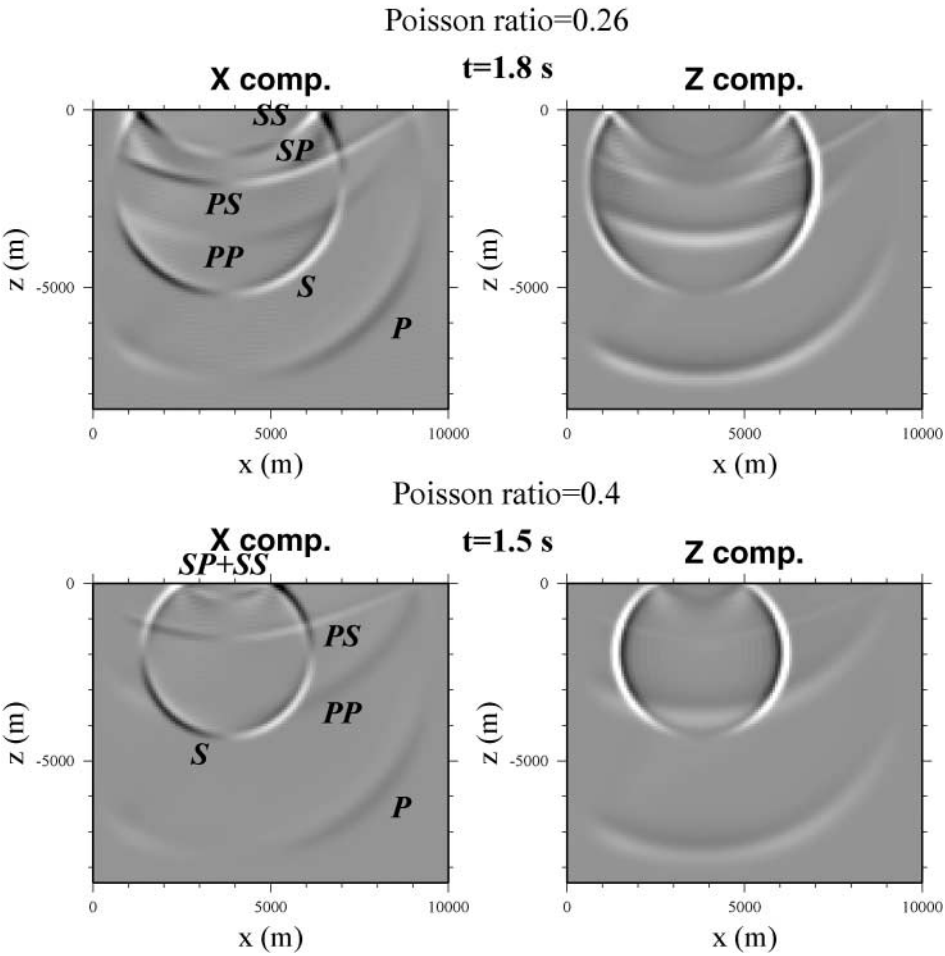

FIG. 9. Snapshots of elastic wave propagation in a homogeneous media with a planar free surface (Lamb's problem). The wavefields are computed for two different Poisson ratios (ν =0.26, 0.4).

In both cases, the wavefields are stable and clear reflected phases from the free surface are generated (*PP*, *PS*, *SP*, *SS* in Fig. 9).

In Fig. 10 we display the calculated displacement seismograms at two receivers (R_1,R_2 in Fig. 8) located at $x = 4453$, 7578 m on the free surface. The numerical responses for the wavelet method are compared with analytic solutions based on Cagniard's technique [13, 59]. For each of the values of Poisson ratios there is a good match with the analytic solutions up to the time when there is a small wave reflection from the artificial boundary (about 3.5 s), indicating the successful implementation of the free-surface boundary condition. For the larger Poisson ratio a very slight time shift can be seen between the numerical and analytic solutions for the large amplitude Rayleigh wave at 2.5 s but the amplitude and pulse shape are well represented.

Here, we note that adjustment of the absorbing boundary conditions may be needed to avoid spoiling the main wavefield by the effect of spurious waves from absorbing boundaries. In particular, spurious waves from surface waves (e.g., Rayleigh waves) tend to become dominant, since surface waves experience low order of geometrical spreading effect compared to body waves (i.e., in 2-D elastic medium with a line source, surface waves do not decay with propagation distance (r), while body waves decay as $\sqrt{1/r}$).

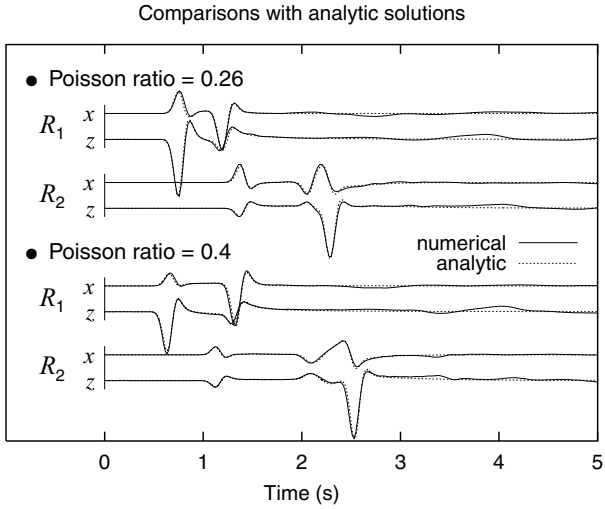

FIG. 10. Comparison between numerical results and analytic solutions for Lamb's problem at two receivers (R_1, R_2 in Fig. 8) placed on a free surface for two different Poisson ratios ($\nu = 0.26, 0.4$).

Therefore, the absorbing region should be designed to give sufficient attenuation of the surface waves by suitable modulation of the attenuation factors (Q_x, Q_z in (68)). We can use, for instance, extension of the effective absorbing region by adjusting B_x and B_z in Q_x and Q_z, or enhancement of attenuation rate in the region by modulating A_x and A_z.

6.3. Two-Layered Heterogeneous Medium

The formulation of the wavelet method is based on a fully heterogeneous medium and so we can introduce particular cases by simply specifying the material parameters. We therefore consider a further case where an analytic solution can be obtained for 2-D propagation of *SH* waves in a two layer medium where the velocity in bottom layer is twice of that in top layer and the density in bottom layer is 1.5 times of that in top layer (Fig. 11). The

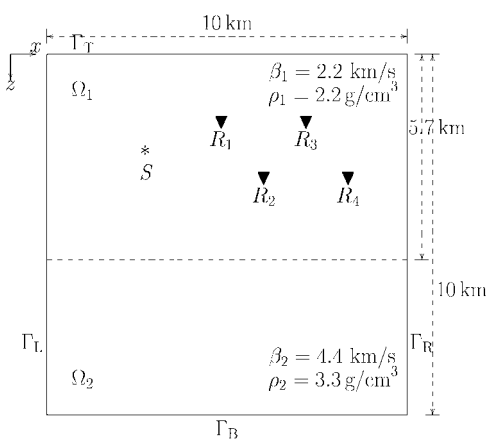

FIG. 11. Description of a two-layered medium for modelling of *SH* wave propagation. The bottom layer has twice the velocity and 1.5 times the density of those in top layer. Four receivers (R_j, $j = 1, 2, 3, 4$) are placed inside the top layer and numerical responses from the receivers are compared with analytic solutions.

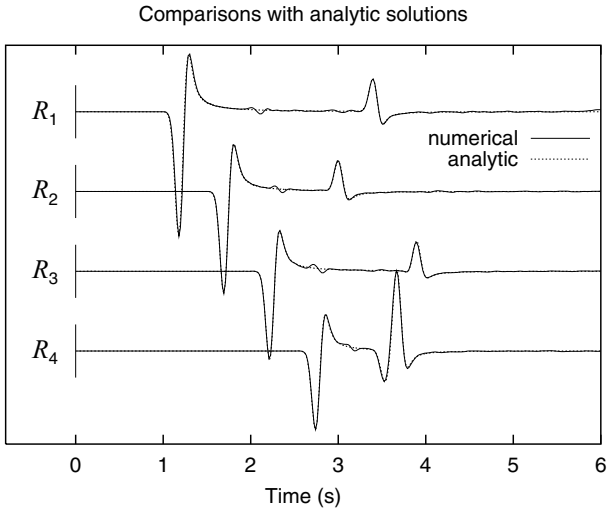

FIG. 12. Comparison between numerical results and analytic solutions for *SH* waves in a two-layered medium. The numerical responses are collected by four receivers (R_j, $j = 1, 2, 3, 4$) in Fig. 11.

displacement in *SH* waves lies along y axis (i.e., normal to the x-z plane where *SH* waves are propagating), and reflection and transmission without conversion of wavetype occur at the interface. The governing *SH* wave equation is given by

$$\frac{\partial^2 u_y}{\partial t^2} = \frac{1}{\rho}\frac{\partial}{\partial x}\left(\mu\frac{\partial u_y}{\partial x}\right) + \frac{\partial}{\partial z}\left(\mu\frac{\partial u_y}{\partial z}\right) + \frac{f_y}{\rho}, \tag{69}$$

where ρ is the density, μ is the shear modulus, and f_y is the body force imposed normal to the x-z plane. Following the same approach as in Sections 4.2, 5.1, 5.2, we are able to implement a wavelet scheme for the *SH* waves; further details can be found in [34].

A point force is applied at (2734 m, 2656 m) (S in Fig. 11) and the internal boundary is located at depth 5703 m with four artificial but absorbing boundaries (Γ_T, Γ_B, Γ_R, Γ_L). The *SH* displacements at four receivers (R_j, $j = 1, 2, 3, 4$) collecting numerical responses placed at (4844 m, 1875 m), (6016 m, 3438 m), (7188 m, 1875 m), (8359 m, 3438 m) are compared with analytic solutions [1] based on the Cagniard technique (see Fig. 12). There is very good agreement between the numerical and analytic results for both the direct waves and those interacting with the interface between the two layers. The pattern of the wavefield can be seen in the snapshot at 3.0 s (Fig. 13) with a direct wave (S), reflected wave (SS_r), transmitted wave (SS_t), interface wave on the internal boundary (I), and head wave (H) connecting transmitted wave and reflected wave.

The comparisons with the analytic solutions in the homogeneous half-space and layered medium case indicate the successful implementation of the wavelet representation for both the main propagation and the boundary conditions.

As an alternative two layer case we undertake a stability test of the method for two-layered medium where a fluid layer $\nu = 0.5$ overlies a solid layer (Fig. 14). Many numerical methods have difficulty in treating this problem with a large contrast in Poisson ratio due to the large discrepancy between two elastic wave speeds (α, β). The incident P wave from an explosive point source inside the solid layer gives rise to both P and S reflected waves (PPr, PSr) from the interface, but only P wave (PPt) transmit to the fluid layer (see Fig. 15). This behaviour

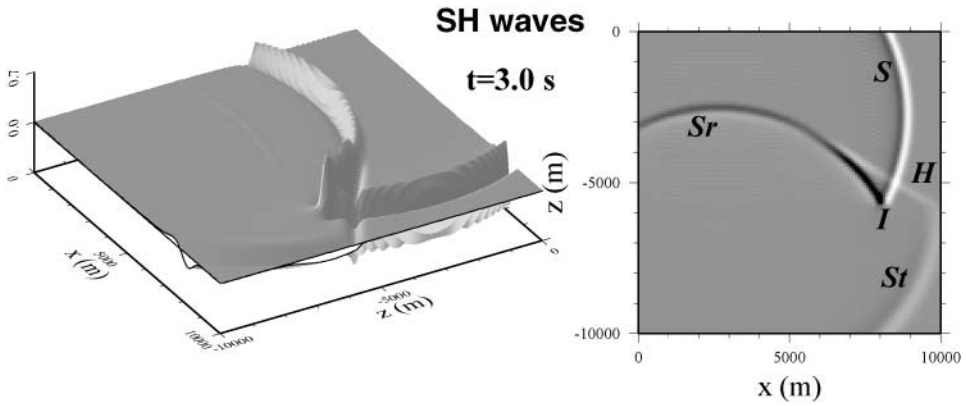

FIG. 13. Snapshot of *SH* wave propagation in a two-layered medium at $t = 3.0$ s. Direct wave (S), reflected wave (S_r), transmitted wave (S_t), interface wave (I) developing on a boundary, and head waves (H) connecting transmitted wave and reflected wave are displayed.

is correctly reproduced with the wavelet treatment using an elastic representation for the whole medium.

For more general problems we need to be able to handle the case of nonplanar boundaries. Boore [11] has suggested two approaches to representing an internal boundary which passes between grid points in finite difference modelling for *SH* waves. These are, first, the modification of the physical parameters at grid points near the boundary and, second, the implementation of explicit boundary condition (i.e., continuity of stress over the boundary). However, as noted by Boore, both approaches need additional computation and also may lead to instability. For a stable treatment with the wavelet-based method, a grid generation technique (Section 5.4) can be implemented by adjusting the grid system to be locally parallel to the boundaries (e.g., [44]). In next section, we consider some topography problems using the grid generation technique.

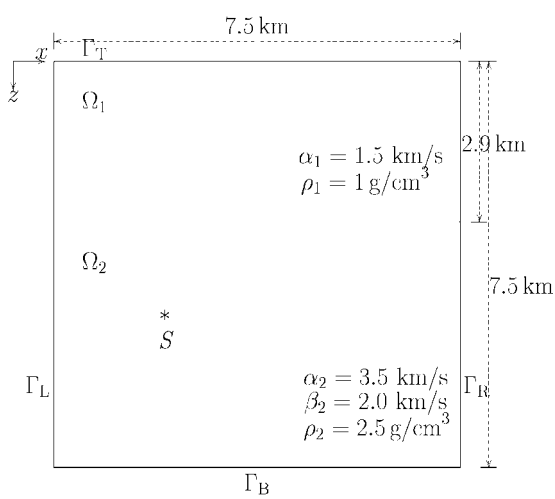

FIG. 14. Description of a fluid-solid configurational medium. An explosive point source is applied inside the solid layer (S).

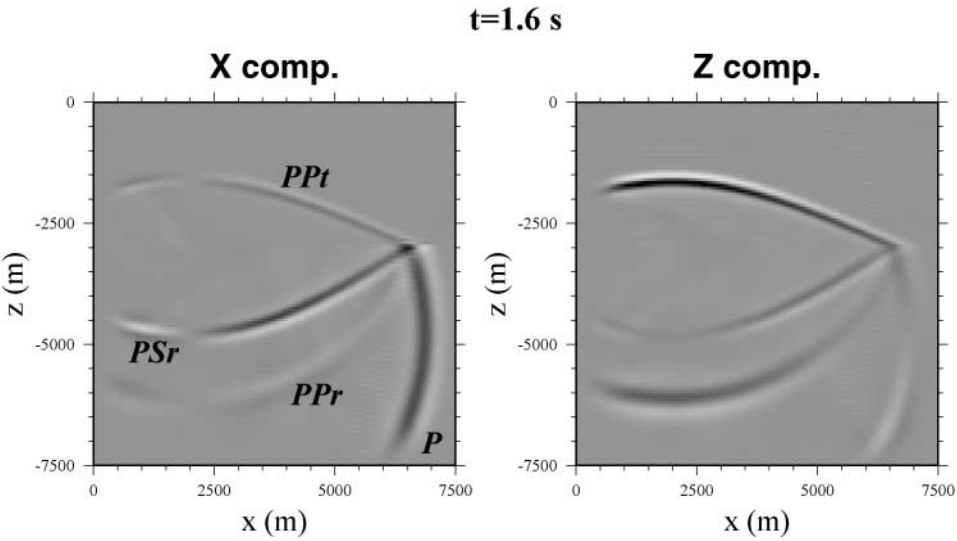

FIG. 15. Snapshots of elastic wave propagation in a fluid-solid configurational medium at $t = 1.6$ s. Incident P wave is reflected as P and S waves (PP_r, PS_r) due to phase coupling on the boundary, and only P wave (PP_t) propagates into the fluid layer.

6.4. Media with Surface Topography

We are able to adapt the wavelet-method for handling elastic wave propagation by using a remapping of the material grid and to make comparison with analytic solutions derived by coordinate transformations.

6.4.1. *Validation Tests for Surface Topography*

We introduce an unbounded elastic medium with a sinusoidal internal topography (see Fig. 16); i.e., the internal horizontal grids are set to be sinusoidal. For this purpose, we consider four artificial boundaries (Γ_T, Γ_B, Γ_L, Γ_R) with absorbing boundary conditions. The material properties are as in Section 6.2 with a Poisson ratio of 0.26. The period of sinusoidal topography is 5 km and the amplitude is 1 km. A vertically directed point force (S_1 in Fig. 16) is applied at (3125 m, 3125 m) from the left and bottom boundaries and four receivers (R_j, $j = 1, 2, 3, 4$) at (3906 m, 5469 m), (4688 m, 5469 m), (6250 m, 7813 m), (7031 m, 7813 m) from the left and bottom boundaries record the numerical response. As we see in Fig. 17 a good match is achieved between the numerical seismograms using the grid-remapping and the analytic solutions [59] for an unbounded domain. The ripples in the numerical solution at later time in the shear wave portion of the response arise from the discretization of the sinusoidal grids and could be reduced by finer discretization of the medium.

Next, we consider the more difficult problem of an elastic medium with topography at the free surface. We introduce a model where analytic solutions can be obtained: a homogeneous medium with an inclined free surface and a point force which is normal to the topography. The analytic solutions can be computed from those of Lamb's problem for a planar surface as in Section 6.2 via suitable rotation of a coordinate system.

The point force normal to the surface is introduced at (3750 m, 2000 m) from the left and top boundaries and four receivers (R_j, $j = 1, 2, 3, 4$) are placed on the free surface at

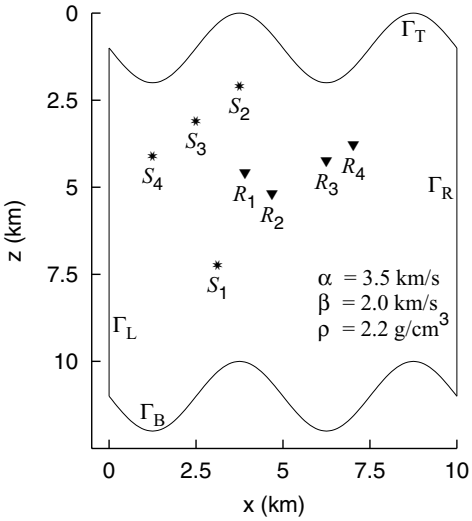

FIG. 16. Description of a 2-D homogeneous elastic medium with a topography. For an accuracy test in an unbounded medium with a vertically directed point force at S_1, four artificial boundaries (Γ_T, Γ_B, Γ_L, Γ_R) are treated as absorbing boundaries and numerical results from four receivers (R_1, R_2, R_3, R_4) are compared with analytic solutions (Section 6.4.1). In numerical modelling of seismic wave propagation in the medium for characteristic three different point-force positions (S_2, S_3, S_4), the top boundary (Γ_T) is considered a free surface (Section 6.4.2).

distance $x = 4453, 5234, 6797, 7578$ m from left boundary (see Fig. 18). In the numerical model we need to have periodicity and so the slanted boundary has to be connected at each end with a hill and valley structure. The comparisons between the numerical and analytic results at the four receivers in Fig. 19 exhibit a good match for the time window before any interaction occurs with the edges of the topography. The more distant receivers (R_3, R_4) display some amplitude discrepancy in the S waves due to effects of reflected waves

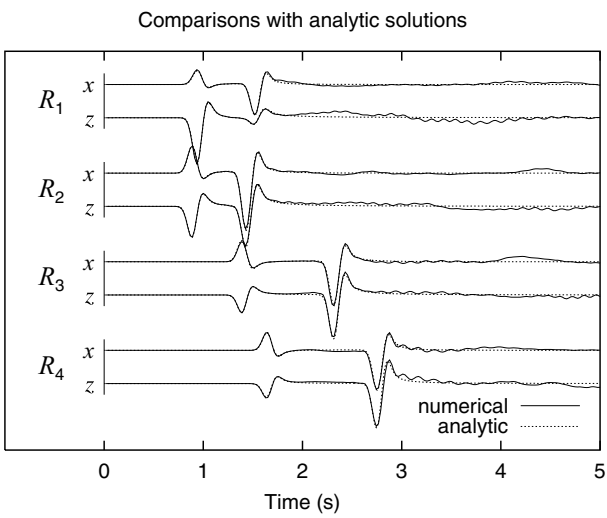

FIG. 17. Comparisons with analytic solutions in a homogeneous unbounded medium represented by a sinusoidal topographic grid systems.

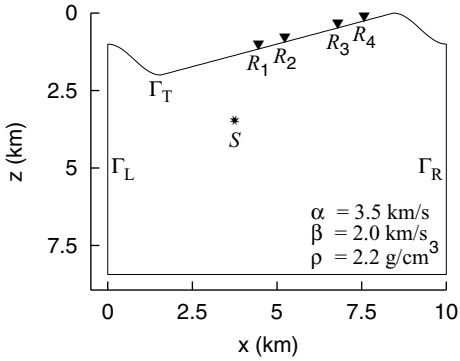

FIG. 18. Description of a homogeneous elastic medium with a inclined free surface. A point force (S) normal to the free surface is applied at depth 2 km and four receivers (R_1, R_2, R_3, R_4) on a free surface record numerical responses to be compared with analytic solutions.

from the hill near right boundary Γ_R (see Fig. 20) which are not included in the analytic results.

6.4.2. *Elastic Wave Propagation in Media with a Sinusoidal Surface Topography*

The results of our validation tests of the wavelet-based method for the topographic-media scheme indicate that the method can be expected to generate accurate responses in complex-topography problems with sufficiently fine discretization. However, it is also important to check the stability of the method with regard to the discrete representation of the topography. We therefore consider two cases of sinusoidal topography: with low-frequency and high-frequency variations.

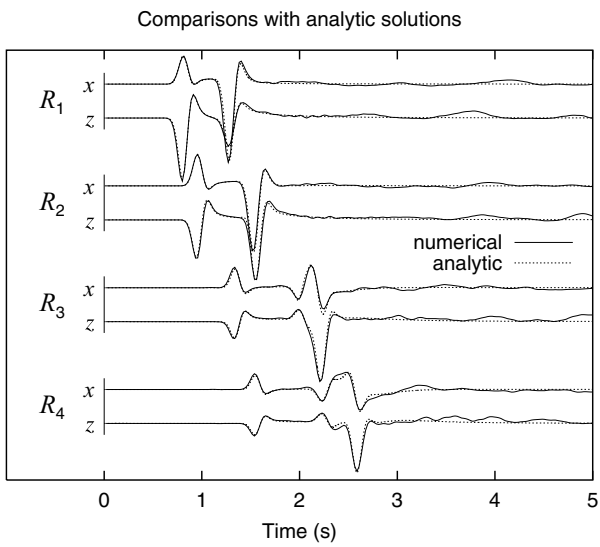

FIG. 19. Comparisons of numerical responses with analytic solutions at four receivers (R_j, $j = 1, 2, 3, 4$, in Fig. 18) in a homogeneous inclined topographic medium.

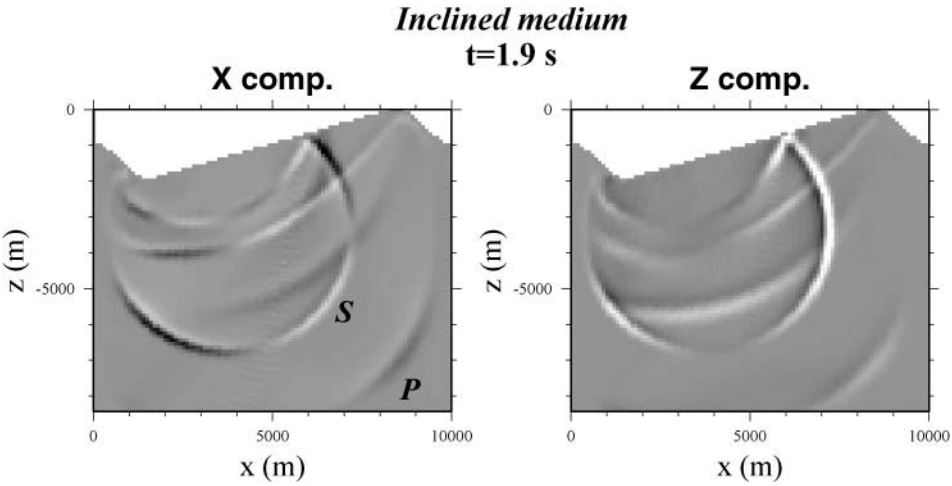

FIG. 20. Snapshots of elastic wave propagation in a homogeneous medium with a inclined free surface at $t = 1.9$ s.

First, we consider the case with long wavelength surface topography, with the same form and material properties as in Section 6.4.1, and implement point forces at three different positions: sources beneath the crest (S_2 in Fig. 16), on the side of the hill (S_3), and in a trough (S_4). All point forces are applied at (3750 m, 2000 m) from left and top boundaries (i.e., the sinusoidal topography is shifted relative to the point-force positions). The top boundary (Γ_T) is considered a free surface in these examples. We see from Fig. 21, that the position of source has a very strong influence on the character of the elastic wavefield. The main *P* and *S* phases are well developed in all cases but the secondary phases are rather different. Internal reflected waves can be generated inside the "hills", and there is also the possibility of body waves produced by conversion from the Rayleigh waves propagating along the sinusoidal free-boundary. The influence of the discretization is minor at this scale.

For the case with high-frequency surface topography we consider a sinusoidal surface with 1428 m wavelength and an amplitude of 250 m. This leads to 9.1 grid points each period of the topography for the 128×128 grid system. Figure 22 shows snapshots of elastic wave propagation in the medium at $t = 1.4, 2.4$ s, and the wavefields generated are stable throughout domain as would be expected from the analysis in Section 5.6. The effect of the topography is to produce a complex pattern of scattered phases following the *S* wave. There is now some influence from the coarse discretization of the surface, the small stair steps lead to irregularities in the coda.

6.5. Application to a Complex Heterogeneous Medium Problem

Our final example is more complex, with elastic wave propagation in a medium containing a fluid-filled crack (Fig. 23). Such a feature with a high contrast over a narrow interval presents a major challenge to traditional grid based methods because of the rapid variations in the medium. Hong and Kennett [35] have demonstrated that the wavelet-based method can give accurate responses in a medium with highly and abruptly varying physical parameters by comparing results of numerical differentiation by the wavelet-based method with those achieved with a fourth-order finite difference method. The wavelet method can

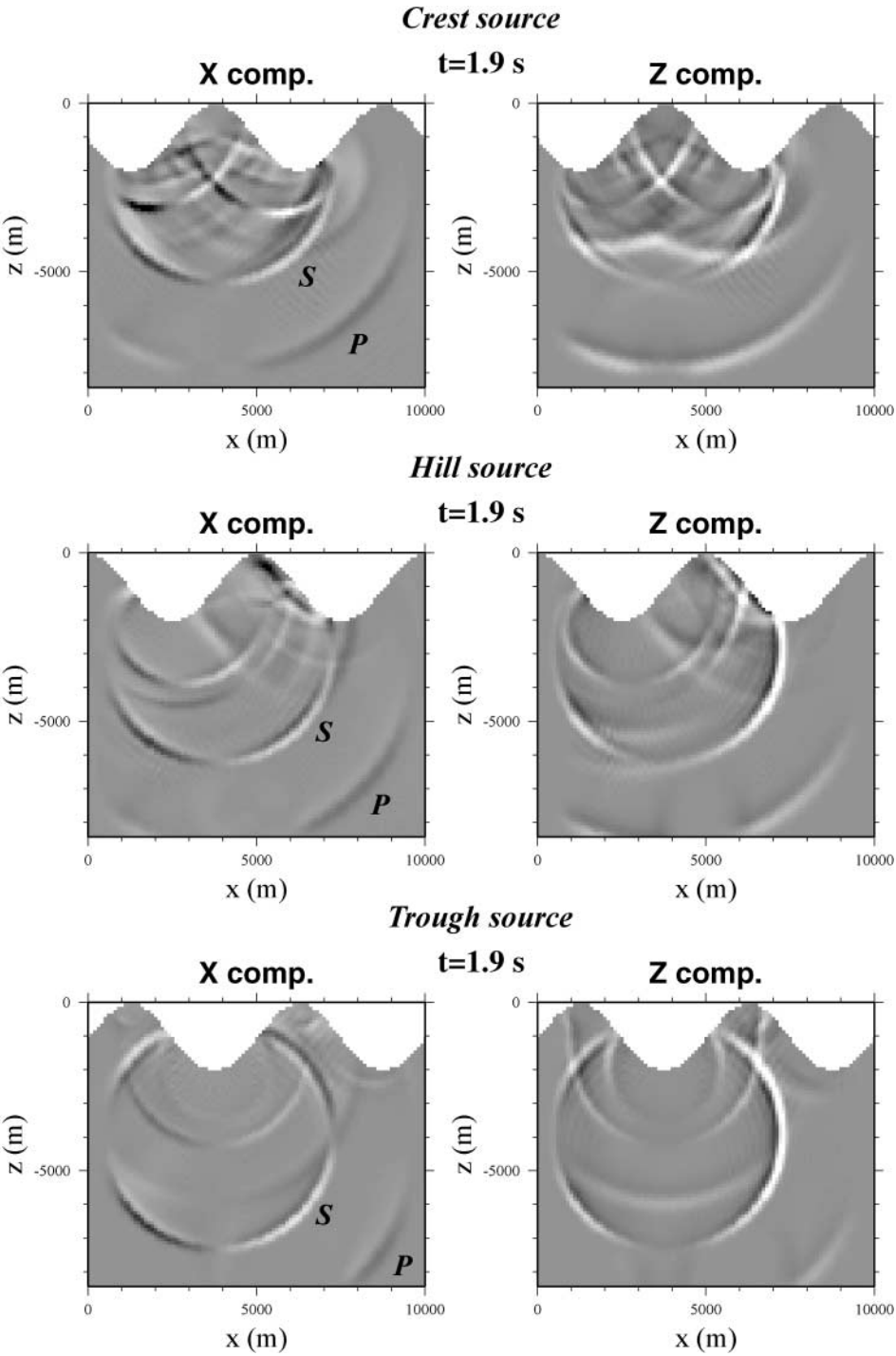

FIG. 21. Snapshots of elastic wave propagation in a medium with a 4π sinusoidal topographic surface at $t = 1.9$ s. Vertically directed point forces are applied at three characteristic positions: beneath crest, hill, and trough.

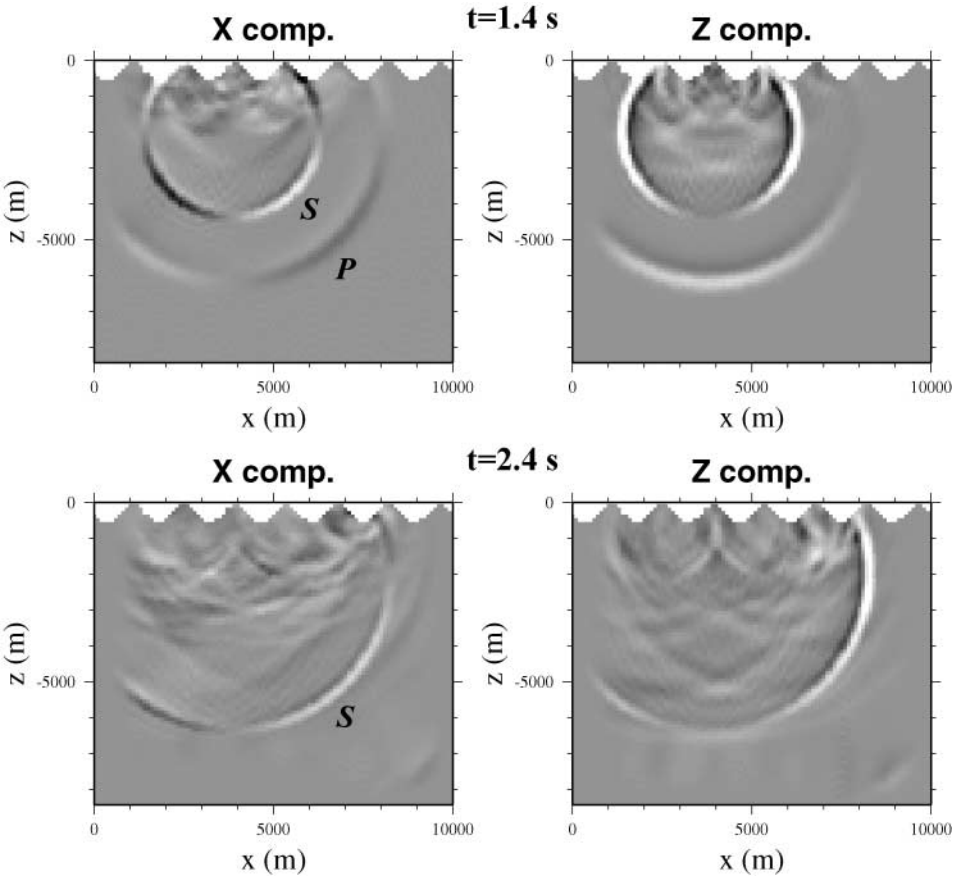

FIG. 22. Snapshots of elastic wave propagation in a medium with a highly varying (14π) sinusoidal topography at $t = 1.4$, 2.4 s.

achieve accurate differentiation even when the higher order finite difference method is having difficulties.

In applications to seismology we need to take account of the complex nature of the 'real' Earth with both mixtures of materials and strong local variations in seismic wave speeds. Scattered waves are a major feature of observed seismograms and the most effective quantitative way of simulating such effects is to introduce some form of stochastic representation of wave speed superimposed on a long wavelength structure (e.g., [26]).

We therefore compare the results for the fluid-filled crack problem with a homogeneous background medium and a heterogeneous medium where the variations in wave speed are based on the Von Karman autocorrelation function (see [63]) with 10% standard deviation. For more details on the generation of a stochastic heterogeneous medium, we refer to [26, 35].

A compressional point force (S in Fig. 23) is applied at (3750 m, 1500 m) and four artificial boundaries are considered as absorbing boundaries. A compressional wave velocity in main medium is 3.15 km/s, a shear wave velocity is 1.8 km/s, and density is 2.2 g/cm^3. The crack is filled with fluid and the compressional wave velocity and density are half of those of main medium.

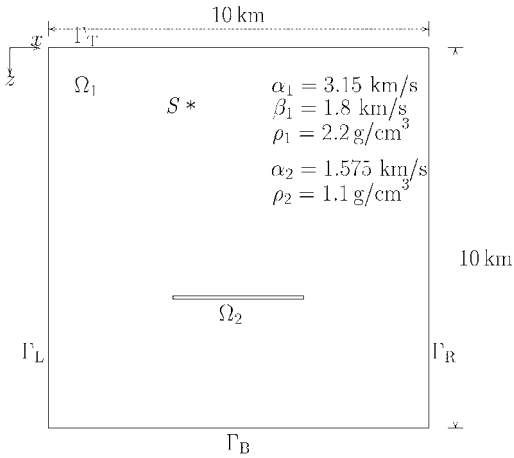

FIG. 23. Description of a medium with a fluid-filled crack. The compressional wave velocity and density in the crack are half of those in reference medium. The reference medium is considered homogeneous or stochastic heterogeneous with a standard deviation by 10%. Four artificial boundaries (Γ_T, Γ_B, Γ_R, Γ_L) are treated as absorbing boundaries.

Figure 24 shows snapshots of the elastic wave propagation for this crack problem at $t = 1.5$ s. Reflected phases (PP_r, PS_r) from the surface of crack, transmitted phases (PP_t, PS_t) through the crack, and diffracted phases (PP_d, PS_d) from both ends of the crack can be seen clearly in the results for the homogeneous background in the left panel of Fig. 24. For the perturbed medium in the right panel, the generated phases are mixed with scattered waves arising form the whole domain through which the P wavefront has passed, and the wavefield displays a more complex shape. Such a combination of a clear initial phase and a complex coda fits well with the nature of observed seismograms.

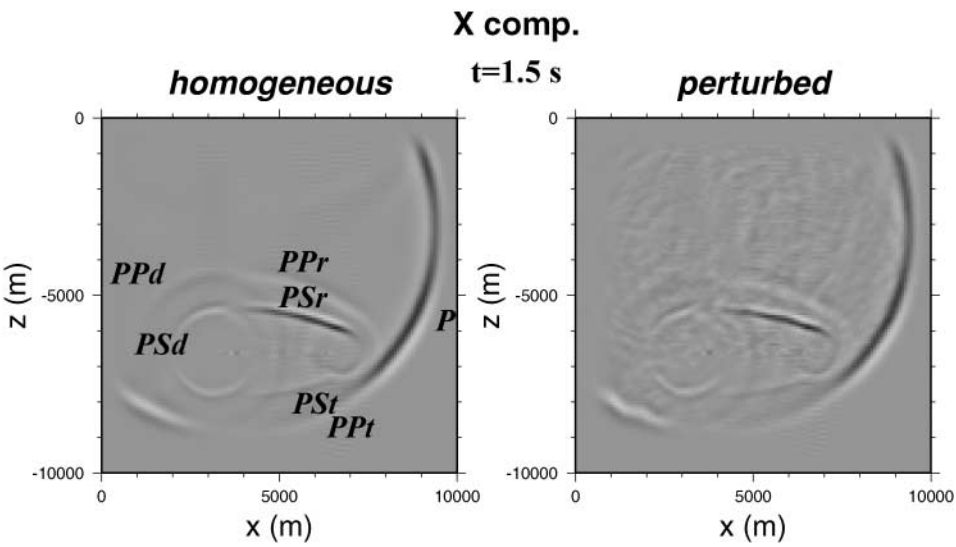

FIG. 24. Snapshots of elastic wave propagation in a complex medium with a fluid-filled crack for two cases; the reference medium is considered homogeneous or stochastic heterogeneous.

7. DISCUSSION AND CONCLUSIONS

We have introduced a wavelet-based method for acoustic and elastic wave equations to simulation of wave propagation in 1-D and 2-D media and have been able to to establish both suitable equation systems and a systematic treatment of boundary conditions.

We use a displacement-velocity formulation scheme for wave equations with treatment of derivatives as linear operators. Discrete time representations are obtained from a semi-group approach applied to a system of first-order partial differential equations in time. The numerical solution uses a recursive explicit scheme, derived from a Taylor expansion for the exponential of matrix operator.

The explicit boundary conditions (e.g., rigid boundary conditions, traction-free boundary conditions) were implemented using equivalent force terms and absorbing boundary conditions were considered implicitly by adding attenuation terms to the governing equation system which are activated only on the artificial boundary regions. As periodic boundary conditions are assumed intrinsically in a wavelet-based method, we have had to find ways to implement physical boundary conditions without producing spurious effects. For the acoustic wave case, with rigid boundary conditions at both ends of the 1-D spatial domain, we applied the boundary conditions over an artificial extension of the medium by a band of grid points to achieve sufficient accuracy. A similar approach has been used for elastic wave propagation in 2-D media, to implement the traction-free boundary condition at a free surface.

The use of equivalent force terms to represent boundary conditions can readily be adapted to other classes of problems and we expect that we can include different types of boundary conditions or singular features in the media (e.g., azimuthal anomalies, scattering) which are hard to describe by just controlling the physical parameters.

Comparisons between the numerical responses from the wavelet method and analytic solutions in various types of media (i.e., homogeneous medium with a planar free surface, layered media, medium with surface topography), we have shown that our scheme has high accuracy in simple media.

However, the strength of the approach lies in applications to complex media where we can exploit the high accuracy and compact support of the representation of differential operators. Thus we have demonstrated the accuracy and stability of the wavelet scheme in complex problems with both rapidly varying topographic media problem and stochastic heterogeneous medium as well as the effect of a sharp variation of physical parameters over a narrow region (a crack problem).

The formulation of the wave equations as a set of first-order differential equations for the evolution of the displacement and velocity fields in time can readily be extended to 3-D media problems. Using the separability of the differential operators we expect to be able to make a comparable extension to the 3-D case.

We have here demonstrated the way in which the wavelet projection can provide a means of coping with physical variations as small scales, but have not made use of the other commonly exploited aspect of wavelets, i.e., their adaptivity. The difficulty of taking an adaptive approach, especially with elastic waves, arises from the multiplicity of possible waves, which becomes most severe for highly heterogeneous media. For some simple problems it may well be possible to make some adaptive grid refinement. But for the complex problems needed for seismological applications, it is difficult to see how adaptivity can be introduced in a systematic way.

APPENDIX A

Formulation of Matrix Operators in *NS*-Form

The construction of a matrix operator in *NS*-form based on the work of Beylkin [7] is described briefly. The operator T on $\mathbf{L}^2(\mathbb{R})$ in *NS*-form is obtained by through the use of operators (A_j, B_j, Γ_j), for each level j ($j \in \mathbb{Z}$), in subspaces which project the subspaces produced by the action of T onto the subspaces $(\mathbf{W}_j, \mathbf{V}_j)$,

$$T = \{A_j, B_j, \Gamma_j\}_{j\in\mathbb{Z}}, \tag{A.1}$$

where each operator is specified by

$$\begin{aligned} A_j &= Q_j T Q_j\colon \quad \mathbf{W}_j \to \mathbf{W}_j, \\ B_j &= Q_j T P_j\colon \quad \mathbf{V}_j \to \mathbf{W}_j, \\ \Gamma_j &= P_j T Q_j\colon \quad \mathbf{W}_j \to \mathbf{V}_j. \end{aligned} \tag{A.2}$$

Here, P_j is a projector onto the scaling subspace $\mathbf{V}_j$ and Q_j onto the wavelet subspace $\mathbf{W}_j$. Expression (A.2) means that the distorted space due to an operation of T on $\mathbf{L}^2(\mathbb{R})$ space can be reorganized into subspaces $\mathbf{V}_j$ and $\mathbf{W}_j$.

Along the discussion in Section 2, the physical space where data are collected is identified as $\mathbf{V}_0$, and the operator T implemented on the space $\mathbf{V}_0$ as T_0. Therefore, considering (A.1) T_0 can be expressed with a set of operators in subspaces $(A_j, B_j, \Gamma_j, j > 0)$ up to a scale N where T_N becomes a null space as

$$T_0 = \{A_j, B_j, \Gamma_j\}_{j=1}^{N}. \tag{A.3}$$

Therefore, when T_0 is decomposed up to a certain scale J which is less than N, we can express T_0 generally as

$$T_0 = \left\{\{A_j, B_j, \Gamma_j\}_{j=1}^{J}, T_J\right\}, \tag{A.4}$$

where T_J is the operator on the scaling subspace of coarsest scale $(\mathbf{V}_J)$, which corresponds to

$$T_J = P_J T P_J\colon \ \mathbf{V}_J \to \mathbf{V}_J. \tag{A.5}$$

Thus, considering (A.3), T_J can be represented through the operator projections on to subspaces of higher scales up to the scale N (i.e., $\{T_J = \{A_j, B_j, \Gamma_j\}_{j=J+1}^{N}\}$). Therefore, considering (A.2) and (A.5), the operator T_0 in (A.4) can be rewritten as

$$T_0 = \sum_{j=1}^{J} (Q_j T Q_j + Q_j T P_j + P_j T Q_j) + P_J T P_J. \tag{A.6}$$

Since the one-dimensional operator (e.g., d/dx in 1-D) is applied for the multi-dimensional operator (e.g., $\partial_x \partial_y$ in 2-D) via separation of operator following directions (see Section 2), we focus on the construction of a homogeneous differential operator with

degree p (d^p/dx^p). When $\mathcal{A}_{il}^j$, $\mathcal{B}_{il}^j$, $\mathcal{C}_{il}^j$, $\mathcal{T}_{il}^j$ are considered as components of matrices A_j, B_j, Γ_j, T_j ($i, l, j \in \mathbb{Z}$), the matrix components can be determined using those for the scale $j = 0$ following relationships as (see [7])

$$\begin{aligned}
\mathcal{A}_{il}^j &= 2^{-pj} \int_{-\infty}^{\infty} \psi(2^{-j}x - i)\psi^{(p)}(2^{-j}x - l)2^{-j}\,dx = 2^{-pj}\mathcal{A}_{il}^0, \\
\mathcal{B}_{il}^j &= 2^{-pj} \int_{-\infty}^{\infty} \psi(2^{-j}x - i)\varphi^{(p)}(2^{-j}x - l)2^{-j}\,dx = 2^{-pj}\mathcal{B}_{il}^0, \\
\mathcal{C}_{il}^j &= 2^{-pj} \int_{-\infty}^{\infty} \varphi(2^{-j}x - i)\psi^{(p)}(2^{-j}x - l)2^{-j}\,dx = 2^{-pj}\mathcal{C}_{il}^0, \\
\mathcal{T}_{il}^j &= 2^{-pj} \int_{-\infty}^{\infty} \varphi(2^{-j}x - i)\varphi^{(p)}(2^{-j}x - l)2^{-j}\,dx = 2^{-pj}\mathcal{T}_{il}^0.
\end{aligned} \tag{A.7}$$

When we set $\alpha_{i-l}^p = \mathcal{A}_{il}^0$, $\beta_{i-l}^p = \mathcal{B}_{il}^0$, $\gamma_{i-l}^p = \mathcal{C}_{il}^0$ and $\tau_{i-l}^p = \mathcal{T}_{il}^0$, the components ($\alpha_{i-l}^p$, β_{i-l}^p, γ_{i-l}^p, τ_{i-l}^p) can be expressed through the wavelet projection theory as

$$\begin{aligned}
\alpha_l^p &= \int_{-\infty}^{\infty} \psi(x - l)\frac{d^p}{dx^p}\psi(x)\,dx, \\
\beta_l^p &= \int_{-\infty}^{\infty} \psi(x - l)\frac{d^p}{dx^p}\varphi(x)\,dx, \\
\gamma_l^p &= \int_{-\infty}^{\infty} \varphi(x - l)\frac{d^p}{dx^p}\psi(x)\,dx, \\
\tau_l^p &= \int_{-\infty}^{\infty} \varphi(x - l)\frac{d^p}{dx^p}\varphi(x)\,dx.
\end{aligned} \tag{A.8}$$

Here, with use of the two-scale difference equations [7, 20], we are led to

$$\begin{aligned}
\alpha_l^p &= 2^p \sum_{k=0}^{L-1}\sum_{k'=0}^{L-1} \left(g_k g_{k'} \tau_{2l+k-k'}^p\right), \\
\beta_l^p &= 2^p \sum_{k=0}^{L-1}\sum_{k'=0}^{L-1} \left(g_k h_{k'} \tau_{2l+k-k'}^p\right), \\
\gamma_l^p &= 2^p \sum_{k=0}^{L-1}\sum_{k'=0}^{L-1} \left(h_k g_{k'} \tau_{2l+k-k'}^p\right),
\end{aligned} \tag{A.9}$$

where the coefficients h_k, g_k are the quadrature mirror filters of length L which is determined by wavelets used in the analysis. For Daubechies wavelets with M vanishing moments, $L = 2M$.

Since α_l^p, β_l^p, and γ_l^p can be expressed in terms of $\tau_{2l+k-k'}^p$ as in (A.9), the differential operator d^p/dx^p can be completely determined by using τ_l^p. Here, the coefficients τ_l^p ($-L + 2 \le l \le L - 2$) are given by [7]

$$\tau_l^p = 2^p \left\{ \tau_{2l}^p + \frac{1}{2}\sum_{k=1}^{L/2} a_{2k-1}\left(\tau_{2l-2k+1}^p + \tau_{2l+2k-1}^p\right) \right\}, \tag{A.10}$$

and

$$\sum_{l=-L+2}^{L-2} l^p \tau_l^p = (-1)^p p!, \tag{A.11}$$

where a_{2k-1} is an autocorrelation of h_i defined by

$$a_n = 2 \sum_{i=0}^{L-n-1} h_i h_{i+n}, \quad n = 1, 2, \ldots, L-1. \tag{A.12}$$

Here the autocorrelation coefficients a_n with even indices are zero ($a_{2k} = 0, k = 1, 2, \ldots, L/2 - 1$), and $a_0 = \sqrt{2}$. The coefficients τ_l^p for d^p/d_x^p ($p = 2, 3, 4$) using Daubechies-6 wavelets are given in Appendix C.

APPENDIX B

Application of a Matrix Operator to a Vector

Using (A.6) and applying a matrix operator of *NS*-form to a vector $f(x)$ (e.g., horizontal (or, vertical) row in a displacement field, pth (or qth) row in Fig. 2), a vector $(T_0 f)(x)$ can be represented in wavelet bases by [7]

$$(T_0 f)(x) = \sum_{j=1}^{J} \left(\sum_{k \in \mathbb{F}_{2^{N-j}}} \hat{d}_k^j \psi_{j,k}(x) + \sum_{l \in \mathbb{F}_{2^{N-j}}} \hat{s}_l^j \varphi_{j,l}(x) \right), \tag{B.1}$$

where N is a maximum number of scale level which can be achievable with a given data set (i.e., $\mathbf{V}_N$ is a null space) in the wavelet expansion, and thereby $J \le N$. The set $\mathbb{F}_{2^{N-j}}$ is composed of positive integers which are less than 2^{N-j}, namely $\mathbb{F}_{2^{N-j}} = \{0, 1, 2, \ldots, 2^{N-j} - 1\}$. Now, in order to obtain a simplified expression for (B.1), an additional multiresolution analysis is applied to the scaling function part $\hat{s}_l^j \varphi_{j,l}(x)$. First, $\hat{s}_l^1 \varphi_{1,l}(x)$ are decomposed into $\tilde{d}_k^2 \psi_{2,k}(x)$ and $\tilde{s}_k^2 \varphi_{2,k}(x)$, and then $d_k^2 \psi_{2,k}(x)$ and $s_k^2 \varphi_{2,k}(x)$ are formulated from the composite sums $(\hat{d}_k^2 + \tilde{d}_k^2)\psi_{2,k}(x)$ and $(\hat{s}_k^2 + \tilde{s}_k^2)\varphi_{2,k}(x)$. Here, $s_k^2 \varphi_{2,k}(x)$ can be additionally decomposed into $d_k^3 \psi_{3,k}(x)$ and $s_k^3 \varphi_{3,k}(x)$ in the wavelet bases. Along this way, we iterate the procedure until $j = J - 1$ and finally we obtain the following expression for $(T_0 f)(x)$ in wavelet bases:

$$(T_0 f)(x) = \sum_{j=1}^{J} \sum_{k \in \mathbb{F}_{2^{N-j}}} d_k^j \psi_{j,k}(x) + \sum_{l \in \mathbb{F}_{2^{N-J}}} s_l^J \varphi_{J,l}(x). \tag{B.2}$$

Through this procedure, the action of a *NS*-form matrix operator on a vector can be represented with a constant accuracy corresponding to level J throughout a computational domain.

APPENDIX C

Coefficients of *NS*-Form of Derivative Operators

The coefficients (τ_l^2) of the nonstandard form (*NS*-form) of second-order derivative operator (∂_x^2) for Daubechies-6 wavelets can be obtained using (A.10) and (A.11) and are given by

$$\begin{aligned}
\tau_0^2 &= \frac{-376411229271430529}{102117402777924000}, & \tau_1^2 &= \frac{39196957859019173888}{16954680029972194125},\\
\tau_2^2 &= \frac{-21387760637407692931}{33909360059944388250}, & \tau_3^2 &= \frac{3474106670623164416}{16954680029972194125},\\
\tau_4^2 &= \frac{-3347641256627152657}{67818720119888776500}, & \tau_5^2 &= \frac{109833452180703232}{16954680029972194125},\\
\tau_6^2 &= \frac{-4455438357648059}{67818720119888776500}, & \tau_7^2 &= \frac{-5266935414784}{96883885885555395},\\
\tau_8^2 &= \frac{-23360548516687}{6739748583342984000}, & \tau_9^2 &= \frac{7077855232}{269121905237653875},\\
\tau_{10}^2 &= \frac{-1511993}{119609735661179500}, & \tau_{-l}^2 &= \tau_l^2 \qquad (l = 1, 2, \ldots, 10),
\end{aligned} \tag{C.1}$$

where the coefficient τ_l^2 satisfies the relationship as

$$\tau_l^2 = \int_{-\infty}^{\infty} \varphi(x-l)\frac{d^2}{dx^2}\varphi(x)\,dx, \quad -10 \le l \le 10. \tag{C.2}$$

where $\varphi(x)$ is a scaling function. In the same way, we can obtain the coefficients (τ_l^3, τ_l^4) for third- and fourth-order of derivative operators:

$$\begin{aligned}
\tau_0^3 &= 0, & \tau_1^3 &= \frac{22116565010234368}{9492080172157275},\\
\tau_2^3 &= \frac{-420791418307754477}{242997252407226240}, & \tau_3^3 &= \frac{7841073309070336}{17085744309883095},\\
\tau_4^3 &= \frac{-11397730655490923}{202497710339355200}, & \tau_5^3 &= \frac{-5044095026176}{632805344810485},\\
\tau_6^3 &= \frac{91367818221882449}{21869752716650361600}, & \tau_7^3 &= \frac{-136220198656}{271202290633065},\\
\tau_8^3 &= \frac{7847540783}{6942778640206464}, & \tau_9^3 &= \frac{44221184}{90400763544355},\\
\tau_{10}^3 &= \frac{-10882557}{23142595467354880}, & \tau_{-j}^3 &= -\tau_j^3 \quad (j = 1, 2, \ldots, 10),
\end{aligned} \tag{C.3}$$

and

$$\begin{aligned}
\tau_0^4 &= \frac{5453233167428123}{141090751716480}, & \tau_1^4 &= \frac{-23559695353083136}{763874147965005},\\
\tau_2^4 &= \frac{382370390316173657}{24443972734880160}, & \tau_3^4 &= \frac{-1244004587271296}{254624715988335},
\end{aligned}$$

$$\begin{aligned}
\tau_4^4 &= \frac{33138229116685523}{48887945469760320}, & \tau_5^4 &= \frac{118758284987008}{763874147965005},\\
\tau_6^4 &= \frac{-1381122434602789}{16295981823253440}, & \tau_7^4 &= \frac{1253534094848}{109124878280715},\\
\tau_8^4 &= \frac{49919995963}{27935968839863040}, & \tau_9^4 &= \frac{-274889216}{12124986475635},\\
\tau_{10}^4 &= \frac{3758251}{86222126048960}, & \tau_{-j}^4 &= \tau_j^4 \quad (j = 1, 2, \ldots, 10).
\end{aligned} \tag{C.4}$$

ACKNOWLEDGMENTS

The authors thank the associate editor, Dr A. Bayliss, and three anonymous reviewers for fruitful comments and reviews. The authors also are grateful to Dr. T. Furumura, Dr. M. Bouchon, and Dr. E. Tessmer for access to their codes and discussions and to Tae-Seob Kang for kind comments and information on finite difference methods. The Alpha Server in the Australian National University Supercomputer Facility was used in the preparation of numerical results.

REFERENCES

1. K. Aki and P. G. Richards, *Quantitative Seismology, Theory and Methods*, Vol. 1 (Freeman, San Francisco, 1980).
2. K. S. Anant and F. U. Dowla, Wavelet transform methods for phase identification in three-component seismograms, *Bull. Seism. Soc. Am.* **87**, 1598 (1997).
3. J. M. Augenbaum, The pseudospectral method for limited-area elastic wave calculations in *Computational Methods in Geosciences*, edited by W. E. Fitzgibbon and M. F. Wheeler (SIAM, Philadelphia, 1992).
4. A. Bayliss, K. E. Jordan, B. J. LeMesurier, and E. Turkel, A fourth-order accurate finite-difference scheme for the computation of elastic waves, *Bull. Seism. Soc. Am.* **76**(4), 1115 (1986).
5. L. K. Bear, G. L. Pavlis, and G. H. R. Bokelmann, multi-wavelet analysis of three-component seismic arrays: Application to measure effective anisotrophy at Piñon Flats, California, *Bull. Seism. Soc. Am.* **89**, 693 (1999).
6. A. Belleni-Morante, *Applied Semigroups and Evolution Equations* (Oxford University Press, Great Britain, 1979).
7. G. Beylkin, On the representation of operators in bases of compactly supported wavelets, *SIAM J. Numer. Anal.* **6**(6), 1716 (1992).
8. G. Beylkin, Wavelets and fast numerical algorithms, *Proceedings of Symposia in Applied Mathematics*, **47**, 89 (1993).
9. G. Beylkin and J. M. Keiser, On the adaptive numerical solution of nonlinear partial differential equations in wavelet bases, *J. Comput. Phys.* **132**, 233 (1997).
10. G. Beylkin, J. M. Keiser, and L. Vozovoi, A new class of time discretization schemes for the solution of nonlinear PDEs, *J. Comput. Phys.* **147**, 362 (1998).
11. D. M. Boore, Finite difference methods for seismic wave propagation in heterogeneous materials, in *Methods in Computational Physics*, Vol. 11, *Seismlogy: Surface Waves and Earth Oscillations*, edited by B. A. Bolt, pp. 1–37 (Academic Press, New York, 1972).
12. M. Bouchon, A simple method to calculate Green's functions for elastic layered media, *Bull. Seism. Soc. Am.* **71**, 959 (1981).
13. R. Burridge, *Some Mathematical Topics in Seismology* (Courant Institute of Mathematical Sciences, New York University, 1976).
14. W. Cai and J. Wang, Adaptive multiresolution collocation methods for initial boundary value problems of nonlinear PDEs, *SIAM J. Numer. Anal.* **33**, 937 (1996).
15. J. M. Carcione, The wave equation in generalized coordinates, *Geophysics* **59**, 1911 (1994).

16. C. Cerjan, D. Kosloff, R. Kosloff, and M. Reshef, A nonreflecting boundary condition for discrete acoustic and elastic wave equations, *Geophysics* **50**, 705 (1985).
17. R. Clayton and B. Engquist, Absorbing boundary conditions for acoustic and elastic wave equations, *Bull. Seism. Soc. Am.* **67**(6), 1529 (1977).
18. W. Dahmen, Wavelet and multiscale methods for operator equations, *Acta Numerica* **6**, 55 (1997).
19. N. Dai, A. Vafidis, and E. Kanasewich, Composite absorbing boundaries for the numerical simulation of seismic waves, *Bull. Seism. Soc. Am.* **84**(1), 185 (1994).
20. I. Daubechies, *Ten Lectures on Wavelets* (SIAM, Philadelphia, Pennsylvania, 1992).
21. G. Deslauriers and S. Dubuc, Symmetric iterative interpolation process, *Constr. Approx.* **5**, 49 (1989).
22. S. Dubuc, Interpolation through an iterative scheme, *J. Math. Anal. Appl.* **114**, 185 (1986).
23. E. Faccioli, F. Maggio, A. Quarteroni, and A. Tagliani, Spectral-domain decomposition methods for the solution of acoustic and elastic wave equations, *Geophysics* **61**, 1160 (1996).
24. J. H. Ferziger, *Numerical Methods for Engineering Application* (Wiley, New York, 1981), p. 270.
25. A. Frankel, Three-dimensional simulations of ground motions in the San Bernardino Valley, California, for hypothetical earthquakes on the San Andreas Fault, *Bull. Seism. Soc. Am.* **83**, 1020 (1993).
26. A. Frankel and R. W. Clayton, Finite difference simulations of seismic scattering: Implications for the propagation of short-period seismic waves in the crust and models of crustal heterogeneity, *J. Geophys. Res.* **91**, 6465 (1986).
27. J. Fröhlich and K. Schneider, An adaptive wavelet-vaguelette algorithm for the solution of PDEs, *J. Comput. Phys.* **130**, 174 (1997).
28. T. Furumura, B. L. N. Kennett, and M. Furumura, Seismic wavefield calculation for laterally heterogeneous whole earth models using the pseudospectral method, *Geophys. J. Int.* **135**, 845 (1998).
29. D. Givoli, Non-reflecting boundary conditions, *J. Comput. Phys.* **94**, 1 (1991).
30. D. Gottlieb, M. Gunzburger, and E. Turkel, On numerical boundary treatment of hyperbolic systems for finite-difference and finite element methods, *SIAM J. Numer. Anal.* **19**, 671 (1982).
31. R. W. Graves, Simulating seismic wave propagation in 3D elastic media using staggered-grid finite differences, *Bull. Seism. Soc. Am.* **86**, 1091 (1996).
32. J. D. Hoffman, *Numerical Methods for Engineers and Scientists* (McGraw-Hill, New York, 1992).
33. M. Holmström, Solving hyperbolic PDEs using interpolating wavelets, *SIAM J. Sci. Comput.* **21**(2), 405 (1999).
34. T.-K. Hong and B. L. N. Kennett, A wavelet-based method for simulation of 2-D elastic wave propagation, *Geophys. J. Int.* (2002), in press.
35. T.-K. Hong and B. L. N. Kennett, Scattering attenuation of 2-D elastic waves: Theory and numerical modelling using a wavelet-based method (submitted).
36. L. Jameson, On the spline-based wavelet differentiation matrix, *Appl. Numer. Math.* **17**, 33 (1995).
37. R.-S. Jih, K. L. McLaughlin, and Z. A. Der, Free-boundary conditions of arbitrary polygonal topography in a two-dimensional explicit elastic finite-difference scheme, *Geophysics* **53**, 1045 (1988).
38. M. Käser and H. Igel, Numerical simulation of 2D wave propagation on unstructured grids using explicit differential operators, *Geophys. Prospect.* **49**, 607 (2001).
39. K. R. Kelly, R. W. Ward, S. Treitel, and R. M. Alford, Synthetic seismograms: A finite-difference approach, *Geophysics* **41**, 2 (1976).
40. B. L. N. Kennett, *Seismic Wave Propagation in Stratified Media* (Cambridge University Press, Cambridge, 1983), p. 342.
41. B. L. N. Kennett, *The Seismic Wavefield*, Vol. I, *Introduction and Theoretical Development* (Cambridge University Press, New York, 2001), p. 370.
42. B. L. N. Kennett, E. R. Engdahl, and R. Buland, Constraints on seismic velocities in the Earth from travel times, *Geophys. J. Int.* **122**, 108 (1995).
43. D. Komatitsch, C. Barnes, and J. Tromp, Wave propagation near a fluid–solid interface: A spectral-element approach, *Geophysics* **66**, 623 (2000).

44. D. Komatitsch, F. Coutel, and P. Mora, Tensorial formulation of the wave equation for modelling curved interfaces, *Geophys. J. Int.* **127**, 156 (1996).
45. D. Komatitsch and J.-P. Vilotte, The spectral element method: An efficient tool to simulate the seismic response of 2D and 3D geological structures, *Bull. Seism. Soc. Am.* **88**, 368 (1998).
46. D. Kosloff and E. Baysal, Forward modeling by a Fourier method, *Geophysics* **47**, 1402 (1982).
47. D. Kosloff, D. Kessler, A. Q. Filho, E. Tessmer, A. Behle, and R. Strahilevitz, Solution of the equations of dynamic elasticity by a Chebychev spectral method, *Geophysics* **55**, 734 (1990).
48. R. Kosloff and D. Kosloff, Absorbing boundaries for wave propagation problems, *J. Comput. Phys.* **63**, 363 (1986).
49. T. Lay and T. C. Wallace, *Modern Global Seismology* (Academic Press, San Diego, 1995), p. 521.
50. A. R. Levander, Fourth-order finite-difference *P-SV* seismograms, *Geophysics* **53**, 1425 (1988).
51. J. Lewalle, Formal improvements in the solution of the wavelet-transformed Poisson and diffusion equations, *J. Math. Phys.* **39**, 4119 (1998).
52. J. M. Lilly and J. Park, Multiwavelet spectral and polarization analysis of seismic records, *Geophys. J. Int.* **122**, 1001 (1995).
53. R. A. Lippert, T. A. Arias, and A. Edelman, Multiscale computation with interpolating wavelets *J. Comput. Phys.* **140**, 278 (1998).
54. K. D. Mahrer, Numerical time step instability and Stacey's and Clayton-Engquist's absorbing boundary conditions, *Bull. Seism. Soc. Am.* **80**(1), 213 (1990).
55. P. Moczo, *Introduction to Modeling Seismic Wave Propagation by the Finite-Difference Method*, Lecture Notes (Disaster Prevention Research Institute, Kyoto University, 1998).
56. P. Moczo, E. Bystricky, J. Kristek, J. M. Carcione, and M. Bouchon, Hybrid modeling of P-SV seismic motion at inhomogeneous viscoelastic topographic structures, *Bull. Seism. Soc. Am.* **87**, 1305 (1997).
57. P. Moczo, J. Kristek, and L. Halada, 3D Fourth-order staggered-grid finite-difference schemes: Stability and grid dispersion, *Bull. Seism. Soc. Am.* **90**, 587 (2000).
58. T. Ohminato and B. A. Chouet, A free-surface boundary condition for including 3D topography in the finite-difference method, *Bull. Seism. Soc. Am.* **87**, 494 (1997).
59. W. L. Pilant, *Elastic Waves in the Earth* (Elsevier, New York, 1979).
60. D. L. Powers, *Boundary Value Problems* (Academic Press, New York, 1972).
61. S. Qian and J. Weiss, Wavelets and the numerical solution of partial differential equations, *J. Comput. Phys.* **106**, 155 (1993).
62. J. W. C. Rosa, F. A. C. M. Cardoso, K. Aki, H. S. Malvar, F. A. V. Artola, and J. W. C. Rosa, Modelling elastic media with the wavelet transform, *Geophys. J. Int.* **146**, 454 (2001).
63. H. Sato and M. C. Fehler, *Seismic Wave Propagation and Scattering in the Heterogeneous Earth* (Springer-Verlag, New York, 1998).
64. N. M. Shapiro, K. B. Olsen, and S. K. Singh, Wave-guide effects in subduction zones: Evidence from three-dimensional modeling, *Geophys. Res. Lett.* **27**, 433 (2000).
65. M. J. Shensa, The discrete wavelet transform: Wedding the À Trous and Mallat algorithms, *IEEE Trans. Signal Processing* **40**(10), 2464 (1992).
66. C. Shin, Sponge boundary condition for frequency-domain modeling, *Geophysics* **60**, 1870 (1995).
67. J. Sochacki, R. Kubichek, J. George, W. R. Fletcher, and S. Smithson, Absorbing boundary conditions and surface waves, *Geophysics* **52**, 60 (1987).
68. R. A. Stephen, F. Cardo-Casas, and C. H. Cheng, Finite-difference synthetic acoustic logs, *Geophysics* **50**, 1588 (1987).
69. G. Strang and T. Nguyen, *Wavelets and Filter Banks* (Wellesley-Cambridge Press, Wellesley, USA, 1996).
70. E. Tessmer, D. Kosloff, and A. Behle, Elastic wave propagation simulation in the presence of surface topography, *Geophys. J. Int.* **108**, 621 (1992).
71. E. Tessmer and D. Kosloff, 3-D Elastic modeling with surface topography by a Chebychev spectral method, *Geophysics* **59**, 464 (1994).

72. K. W. Thompson, Time-dependent boundary conditions for hyperbolic systems, II, *J. Comput. Phys.* **89**, 439 (1990).
73. M. Tibuleac and E. T. Herrin, An automatic method for determination of *Lg* arrival times using wavelet transforms, *Seism. Res. Lett.* **70**, 577 (1999).
74. O. V. Vasilyev, Y. Y. Podladchikov, and D. A. Yuen, Modelling of viscoelastic plume–lithosphere interaction using the adaptive multilevel wavelet collocation method, *Geophys. J. Int.* **147**, 579 (2001).
75. J. Virieux, *P-SV* wave propagation in heterogeneous media: Velocity-stress finite-difference method, *Geophysics* **51**, 889 (1986).
76. K. Yomogida and J. T. Etgen, 3-D wave propagation in the Los Angeles Basin for the Whittier-Narrows earthquake, *Bull. Seism. Soc. Am.* **83**(5), 1325 (1993).
77. J. Zahradnik, Simple elastic finite-difference scheme, *Bull. Seism. Soc. Am.* **85**(6), 1879 (1995).
78. Y.-G. Zhang and J. Ballmann, Two techniques for the absorption of elastic waves using an artificial transition layer, *Wave Motion* **25**, 15 (1997).